Late Quaternary development of the Storfjorden and Kveithola Trough Mouth Fans, northwestern Barents Sea

J. Llopart [a, b], R. Urgeles [a, *], A. Camerlenghi [c], R.G. Lucchi [c], M. Rebesco [c], B. De Mol [a]

[a] Dept. Geociencies Marines, Institut de Ciències del Mar (CSIC), Passeig Marítim de la Barceloneta 37-49, 08003 Barcelona, Spain
[b] Dept. Estratigrafia, Paleontologia i Geociències Marines, Facultat de Geologia, Universitat de Barcelona, Martí i Franqués s/n, E08028 Barcelona, Spain
[c] Istituto Nazionale di Oceanografia e di Geofisica Sperimentale, Borgo Grotta Gigante 42/C, 34010 Sgonico (TS), Italy

ARTICLE INFO

ABSTRACT

The development of two Arctic Trough Mouth Fans (TMFs), the Storfjorden and Kveithola TMFs, is investigated by means of sub-bottom and seismic reflection profiles, multibeam bathymetry and sediment samples allowing their detailed stratigraphic architecture to be defined. We find that the TMFs mainly consist of an alternation of rapidly deposited glacigenic debris flows during glacial maxima and a sequence of well-layered plumites and hemipelagic sediments, which were mainly deposited during the deglaciation phase of the adjacent glacial trough. We have identified eight units above regional reflector R1, which indicate that the ice sheet reached the shelf edge within the Storfjorden Trough on at least three occasions during the last ~200 ka. A shallow subsurface unit of glacigenic debris flows suggests that the ice sheet had a short re-advance over the northern and central part of Storfjorden after the Last Glacial Maximum. From stratigraphy, core and literature data, we estimate that ice sheets reached the shelf edge between 19.5 to 22.5 ka, 61 to 65 ka and 135 to 167 ka. Detailed seismic imaging allows us to refine the sedimentary model of Arctic TMFs. The main differences to previous models involve gully formation during not only the deglaciation phase, but also during interglacials by dense shelf water cascading, and a specific timing for the occurrence of slope failures (i.e., shortly after the deglaciation phase). High mean sedimentation rates during glacial maxima of up to 18 kg m^{-2} yr^{-1} likely allow excess pore pressure to develop in the water rich plumites and hemipelagic sediments deposited in the previous deglacial period, particularly where such plumites attain a significant thickness. The position of the submarine landslides in the stratigraphic record suggest that such excess pore pressure is not enough to trigger the slope failures and suggests that earthquakes related to isostatic rebound are likely involved in the final activation.

1. Introduction

During glacial periods, ice streams provide a strong terrigenous input for the buildup of sedimentary fans located at the mouth of some cross-shelf glacial troughs. Grounding of ice streams near the shelf edge during glacial maxima, induces intense glacially-derived debris flow activity over a few thousand years in Trough Mouth Fans (TMFs) (Vorren and Laberg, 1997; Taylor et al., 2002; Ó Cofaigh et al., 2013). These Glacigenic Debris Flows (GDFs) are interbedded with high density melt-water plume sediments (plumites) deposited during deglaciation periods (Hesse et al., 1997; Landvik et al., 1998; Lucchi et al., 2012). TMFs therefore contain a continuous record of the interplay between past glacial dynamics and glacimarine to marine sedimentary processes.

Glacial troughs are the result of erosion and deposition of till transported subglacially by the ice sheets towards the shelf edge (Fiedler and Faleide, 1996). Through deposition of basal tills and GDF deposits, ice streams induce shelf edge progradation that may attain a few kilometers (Vorren et al., 1990; Rebesco et al., 2011). However not all glacially carved cross-shelf troughs develop a TMF at its mouth. Factors such as distance to the ice sheet interior, size of the drainage basin, number of ice advances and duration of glaciations play a significant role in the development of such sedimentary bodies (Batchelor et al., 2013). TMFs are particularly well-developed in the western margin of the Barents Sea (Sættem et al., 1994; Andersen et al., 1996; Laberg and Vorren, 1996a). The onset of

glacigenic sedimentation, development and major progradation of these TMFs during the Pleistocene was not, however, synchronous (Dahlgren et al., 2005). TMFs are characterized by alternating sedimentation rates (high during glacial maxima, low during interglacials) (Laberg et al., 2010) and contrasting sedimentary deposits, both in terms of facies (Lucchi et al., 2013) and physical properties (Llopart et al., 2014). TMF sedimentation patterns and TMF architecture are therefore not only important to determine past ice extent and climate history, but also for understanding, fluid migration pathways (i.e. high-latitude petroleum systems) and the geohazard from major submarine slope failures. This study aims to determine i) the detailed, recent (last ~200 ka) sedimentary architecture of the Storfjorden and Kveithola TMFs using an extensive and high resolution dataset, ii) provide a better insight into the cycle of sedimentary processes that shape the morphology of TMFs as a tridimensional feature and iii) improve understanding of the relationship between alternating glacigenic to marine sedimentation and the timing of submarine landslides within the climatic cycle.

2. Geological setting

The Barents Sea is an epicontinental sea bounded by two passive continental margins to the north and west. The gradual northward opening of the Norwegian-Greenland Sea began at the Paleocene−Eocene transition. Upper Paleozoic and Mezosoic rocks constitute the Svalbard Platform and the basin province between the Svalbard Platform and the Norwegian coast (Faleide et al., 1993). The western basin province consists of three main segments: (1) a southern sheared margin; (2) a central rifted complex associated with volcanism and (3) a northern initially sheared and later rifted margin along the Hornsund Fault Zone (HFZ; Fig. 1) (Talwani and Eldholm, 1977; Eldholm et al., 1984; Faleide et al., 1993). The basal post-rift sedimentary sequence of Paleogene to Late Pliocene age is overlain by a 3.5−4 km Plio-Pleistocene glacially dominated sequence deposited in three phases: (1) an initial ice growth phase (3.6−2.4 Ma); (2) a transitional growth phase (~2.4−1.0 Ma) and (3) a large scale glacial intensification phase (1.0 Ma to present) (Knies et al., 2009).

Major structures that cross the Storfjorden trough include the Hornsund Fault Zone (HFZ), which together with other tectonic structures south of Spitsbergen, affects the oceanic basement and the Plio-Pleistocene sedimentary cover (Faleide et al., 1993, 2008). These structures were likely active during loading and unloading by ice stream growth and retreat and are still active today (Pirli et al., 2013).

Along the western Barents Sea three main seismic units (GI−GIII) and eight regional seismic reflectors (R7-R1 and R4a) have been identified (Faleide et al., 1996; Knies et al., 2009). R7 marks the onset of extensive glaciation 2.7−2.3 Ma ago (Faleide et al., 1996; Butt et al., 2000; Knies et al., 2009), while R4a, dated at ~1.3 Ma (Raymo et al., 1999), is associated with the full development of cross shelf troughs and TMFs (Rebesco et al., 2014). The shallower GIII sequence above R1 has been described as a succession of glacial/interglacial periods (Laberg and Vorren, 1996b). Based on paleomagnetic polarity of the upper GIII sequence Sættem et al. (1992) suggested a <730 ka age, while the same author using aminoacids analysis suggested a <440 ka age. From the study of sedimentation rates in cores from the Isfjorden TMF, Elverhøi et al. (1995) extrapolated an age of 200 ka for the "Upper Glacial Unit", which base could match with R1. Faleide et al. (1996) and Hjelstuen et al. (1996) suggested an age of 440 Ka while Butt et al. (2000), Knies et al. (2009) and Rebesco et al. (2014) favor the younger 200 ka age.

During the last 200 kyrs the Late Saalian and Weichselian glaciations have affected the Barents and Kara Seas. Ice advance in this area started at 180 ka BP and reached maximum expansion at 155 ka BP (Lambeck et al., 2006). Maximum expansion was followed by retreat and readvance during the Saalian, which ended at 135 ka BP over Scandinavia (Spielhagen, 2004; Lambeck et al., 2006). The Weichselian glaciation comprises three major ice sheet advances during Marine Isotopic Stages (MIS) 5d (90−80 ka), 4 (60−50 ka) and the Last Glacial Maximum (LGM) (20−15 ka) (Mangerud et al., 1998; Svendsen et al., 2004). In the Western Barents Sea, a shift from glacial to interglacial conditions and vice-versa has been influenced, amongst other factors, by the interaction of ice sheets with the West Spitsbergen Current (WSC) and the East Spitsbergen Current (ESC) (Mangerud and Svendsen, 1992; Siegert et al., 2001; Rasmussen et al., 2007). Pedrosa et al. (2011) suggest that the subtle tri-lobulated Storfjorden TMF (lobes labeled I to III in Fig. 1) formed under the influence of an ice stream with three major sub-ice streams with different ice-thickness and source area.

At present, a major control on sediment dynamics on the western Barents Sea is exerted by dense shelf waters produced from sea ice growth and brine release (Quadfasel et al., 1988; Schauer and Fahrbach, 1999). The dense shelf waters are driven in a plume toward the shelf edge, where they cascade into the deep basin (Quadfasel et al., 1988; Schauer and Fahrbach, 1999). Their measured velocity in the northern Storfjorden upper slope reaches the necessary minimum shear velocity to erode sediments (Sternberg et al., 2001; Akimova et al., 2011) and lose their erosive capability at about the middle slope where they turn north influenced by the WSC (Wobus et al., 2013).

3. Data and methods

The data used in this article were collected during two coordinated research cruises within the International Polar Year Activity (IPY) 367: BIO Hespérides cruise SVAIS (2007) and R/V OGS-Explora cruise EGLACOM (2008). Data includes multibeam bathymetry, shallow sub-bottom profiles and single channel (SCS) and multi-channel seismic (MCS) reflection data (Fig. 2). The multibeam bathymetry data acquired during the SVAIS cruise were collected using two hull-mounted multibeam echo sounders: a 12 kHz Simrad EM-120 in deep water and a 95 kHz Simrad EM-1002S in shallow water. During the EGLACOM cruise the hull-mounted 12 kHz Reson MB8150 and 100 kHz MB8111 multi-beam echosounders were used for deep and shallow waters respectively. The total coverage of the multibeam surveys in both cruises is ~15,300 km². Nearly 9500 km of sub-bottom profiles were acquired using the hull mounted parametric TOPAS PS 18 (SVAIS cruise) and a BENTHOS CAP-6600 CHIRP profiler (EGLACOM cruise) with a sweep range of 0.5−6.0 kHz and 2−7 kHz respectively. These profiler systems provided sub-bottom information for up to 200 ms twtt (two way travel time) with a vertical resolution on the decametric scale. The SVAIS SCS data were collected using a 210 cubic inches GI gun and a 10 m ministreamer towed 100 m behind the ship and recorded at a sampling rate of 0.5 ms. Data processing was limited to predictive Wiener deconvolution, bandpass filter (45−550 Hz) and AGC. The EGLACOM MCS data were acquired using a 160 cubic inches array of 4 sleeve air guns and a 1200 m digital streamer with 96 channels (spaced 12.5 m), while recording was performed at a sampling rate of 1 ms. Processing at OGS using the FOCUS software from Paradigm Geophysical included a t-squared scaling for spherical divergence correction, Multi-Channel Shot spiking deconvolution, bandpass filtering following the water bottom and trace equalization. Five piston cores and four gravity cores with lengths ranging between 1.01 and 6.42 m were also collected during the SVAIS and EGLACOM cruises respectively (see Lucchi et al., 2013).
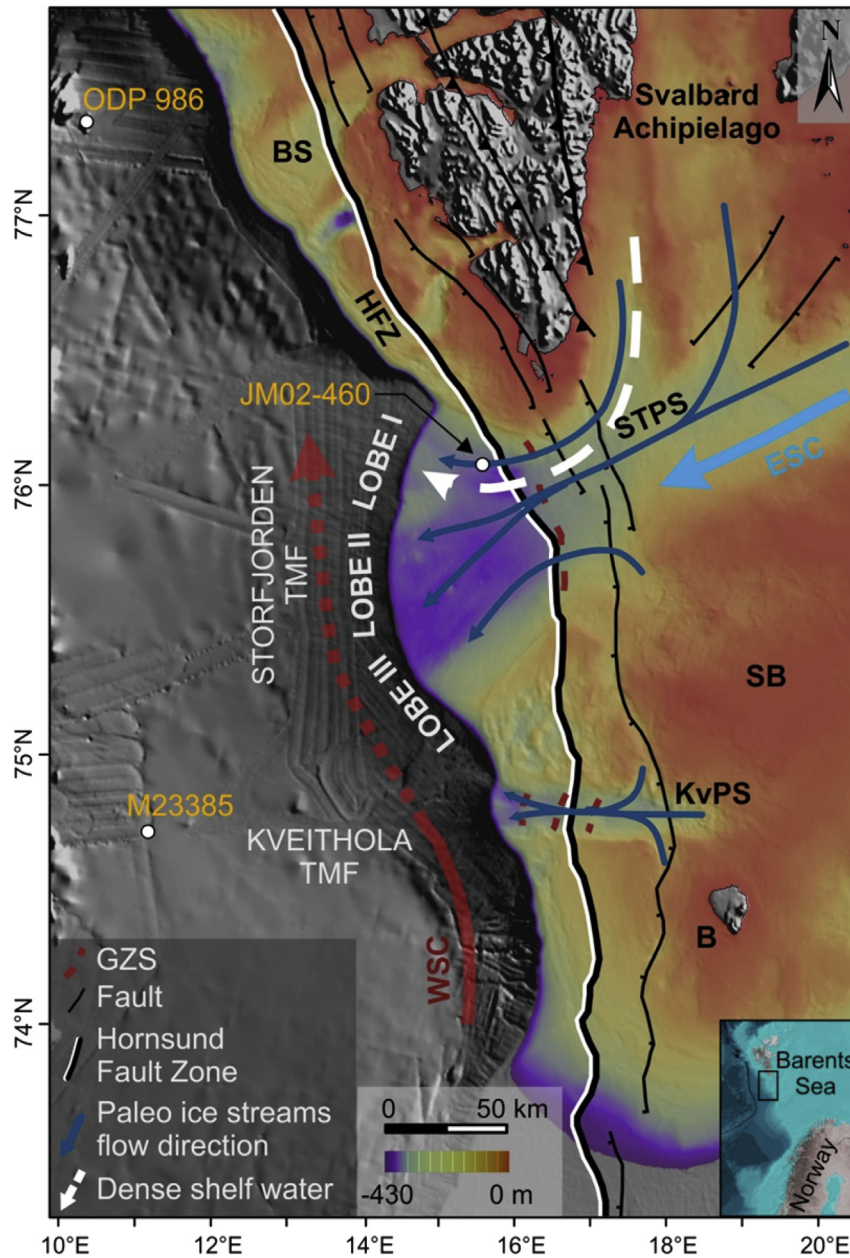
Fig. 1. Map of the study area with inferred direction of the main ice streams present during the LGM indicated by blue lines (Lucchi et al., 2013). White dots correspond to ODP site 986 (Butt et al., 2000), core JM02-460 (Rasmussen et al., 2007) and core M23385 (Dokken and Hald, 1996). Deep red dashed lines indicate Grounding Zone Systems (GZS), black lines are the main tectonic structures in the study area (modified from Pirli et al., 2013) and black-white line depicts the trace of the Hornsund Fault Zone (Faleide et al., 1993). White dashed arrow tentatively marks the cold dense shelf water formed during winters (Ślubowska-Woldengen et al., 2008). Bathymetry from Jakobsson et al. (2012). BS: Bellsund; HFZ: Hornsund Fault Zone; STPS: Storfjorden Paleo-ice stream; SB: Spitsbergen Banken; KvPS: Kveithola Paleo-ice stream; B: Bjørnøya; WSC: West Spitsbergen Current; ESC: Eastern Spitsbergen Current. Inset shows location. (For interpretation of the references to color in this figure legend, the reader is referred to the web version of this article.)

Integrated data interpretation of the sub-bottom profiler, MCS and SCS data was performed using the Kingdom Suite software provided by IHS. Sub-bottom profiler data were used to identify the shallow subsurface structure, while SCS and MCS were used to identify deeper sedimentary units. Reflector R1, which is the deepest reflector of interest, was propagated from ODP Site 986 (Forsberg et al., 1999) and correlated along the entire SVAIS and EGLACOM seismic surveys (see also Rebesco et al., 2013). With the aid of multibeam bathymetric and seismic data, surface and shallow sub-surface features that have a seafloor expression were mapped using GIS tools. Deeper structures were mapped using both Kingdom Suite and GIS tools. Picked reflectors were gridded using Kingdom Suite's flex algorithm with a grid spacing of 80 m.

Volume and thickness calculations from the seismic data have been made using a linear p-wave seismic velocity gradient of $1.48 + 1.5z$ km/s, where z is depth in the sedimentary section. This gradient is consistent with sonic velocity data from ODP Site 986D (Laberg et al., 1996) and implies that the highest velocities at the base of the studied section are ~1.75 km/s. Taking a constant value of 1.5 km/s and a gradient of $1.5 + 2.13z$ km/s (the velocity gradient observed in shallow sediment cores, see Supplementary material), an error is induced into the calculated mean thicknesses (see below) of the deeper units of ±11%.

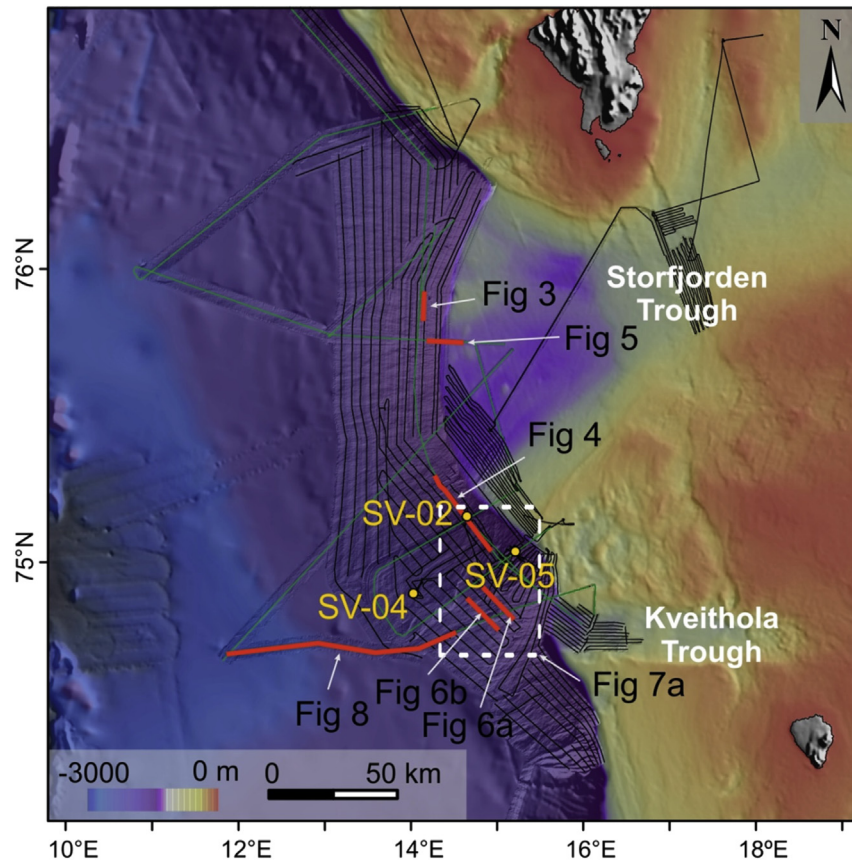The relationship of void ratio (porosity) to depth is highly non-

Fig. 2. Detailed multibeam bathymetry shaded relief of the study area merged with Jakobsson et al. (2012) bathymetric data showing SVAIS cruise cores, sub-bottom profiler (black lines) and seismic (green lines) dataset. The lines shown in Fig. 3, Fig. 4, Fig. 5, Fig. 6 and Fig. 8 are highlighted in red; Fig. 7a is marked with dashed white square. (For interpretation of the references to color in this figure legend, the reader is referred to the web version of this article.)

linear near the seabed surface. This has major implications for determining sedimentation rates between dated levels within an already compacted sequence. Sediment layers may double their thickness when fully decompacted. In this manuscript we adopt a slightly modified version of the iterative forward modeling approach of Tovey and Paul (2001) to objectively compare sedimentation rates between shallow and deeper sedimentary sequences. To this end we use consolidation data measured in plumites and GDF shallow sequences (Table 1), which allow the compression Index (C_c) and initial void ratio (e_0) from the virgin consolidation line to be determined (see Llopart et al. (2014)). In this approach, we also account for the fact that the TMFs present layers of different compression characteristics (plumites and GDFs). Because of the alternating nature of these two sediment types, a double iterative process needs to be carried out to determine the thickness of units with one sediment type or another.

Cores SV-02, SV-04 and SV-05 from the SVAIS cruise have been used to correlate acoustic facies with sedimentary units. On these cores, AMS ^{14}C dating analyses were performed at selected stratigraphic intervals (see Lucchi et al. (2013) for detailed information).

Table 1
Sediment compression characteristics used for decompacting sedimentary units on the Trough Mouth Fan (Llopart et al., 2014).

Predominant sediment type	C_c	e_0
Plumites (Units A, C, E, G)	0.289	1.919
Glacigenic Debris Flows (Units B, D, F)	0.235	1.519

4. Results

4.1. Shallow seismic stratigraphy

The high-resolution seismic stratigraphy of the Storfjorden and Kveithola TMFs is dominated by a sharp alternation of acoustically "laminated" and "transparent" units, although some reflections might be present within the "transparent" units as explained further below. The laminated units have relatively continuous high amplitude reflectors draping pre-existing topography, while the transparent units have a hummocky internal reflector configuration, a basal erosive surface and an irregular upper boundary (see also Lucchi et al., 2012). A similar set of acoustic facies has also been found in other TMFs (Laberg and Vorren, 1995; Ó Cofaigh et al., 2003). Eight seismo-stratigraphic units have been identified above reflector R1. From top to bottom, we have respectively named the stratified units A, C, E and G, while the four transparent units are α, B, D and F (Figs. 3 and 4).

On the shelf, the Storfjorden trough displays a series of stacked transparent units that are more tabular than the transparent units on the TMF. A maximum of three transparent units have been identified on the shelf (T_B, T_D, T_F). No laminated units occur in between these transparent shelf units. The transparent units on the shelf are separated by rather irregular to undulated surfaces (Fig. 5). Changes in slope and limited penetration immediately beyond the shelf edge complicate accurate correlation of shelf and slope units along the whole dataset. Such correlation is only possible along selected SCS/MCS data (Fig. 5).

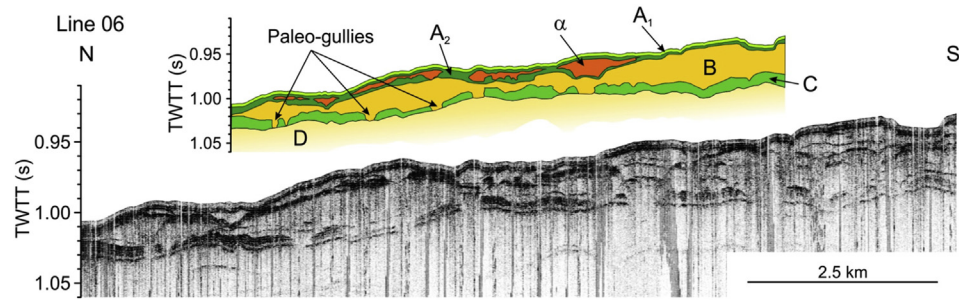Scarps of multiple sizes often disrupt both laminated and

Fig. 3. Top interpreted cross-section. Bottom TOPAS sub-bottom profile Line 06 showing shallow subsurface TMF transparent and laminated units (for location see Fig. 2). Units shown in shades of yellow are interpreted to correspond to Glacial Maxima (GM) periods while units shown in shades of green are interpreted to correspond to Inter-Glacial Maxima (IGM) periods. Bottom of unit D is not completely imaged in this profile. (For interpretation of the references to color in this figure legend, the reader is referred to the web version of this article.)
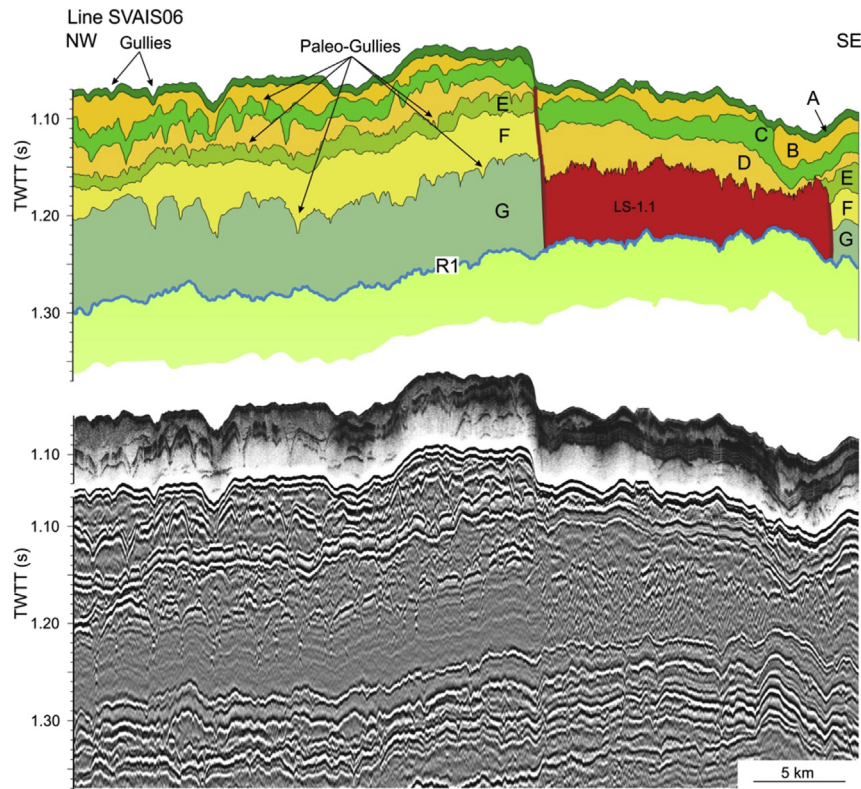

Fig. 4. Top. Interpreted cross-section. Bottom. Airgun seismic reflection and corresponding sub-bottom profile parallel to the shelf edge (for location see Fig. 2) showing gullies and paleo-gullies cutting into IGM sediments (shades of green) while they are filled by younger GM units (shades of yellow). To the south gullies and paleo-gullies disappear and the sequence is interrupted by landslide LS-1.1 (red). The base of this landslide is the regional reflector R1 (Faleide et al., 1996). The unit on top of LS-1.1 is the GM unit D. The sub-bottom profile is displayed at the same horizontal and vertical scale to show matching of acoustic facies between Airgun SCS and TOPAS parametric 3.5 kHz profiles. (For interpretation of the references to color in this figure legend, the reader is referred to the web version of this article.)

transparent units, particularly near the southern limit of the Storfjorden TMF and at the confluence with the Kveithola TMF. Acoustically transparent (in sub-bottom profiles)/chaotic (in SCS and MCS data) sedimentary masses occur associated with these scarps. The chaotic character on seismic reflection data, clearly stands out from that of the transparent more regionally widespread units B, D and F (Fig. 6). Furthermore, the lateral boundaries of these sedimentary masses are sharply cut into the surrounding sediments.

The acoustic character of all laminated units is quite similar. However, we can subdivide unit A into: A_1 and A_2. A_1 corresponds to the uppermost seismo-stratigraphic unit in the studied interval. This uppermost unit is characterized by very low-amplitude

reflections to almost transparent character and is the only unit which can easily be tracked across the slope and shelf. A_2 displays a more parallel laminated character, in a similar way to C, E and G. Sharply cut incisions are evident on these older laminated units which are filled in by the overlying transparent units (e.g. incisions in unit C are filled in by unit B) (Fig. 4). Unit G, which is the thickest and deepest well-laminated unit, has a 60–110 ms twtt more reflective upper part while the remainder of the unit has weaker internal reflections, except for a strong reflector located at about half its thickness.

Transparent units occur mainly in the upper and middle continental slope in the northern and central parts of the Storf- jorden TMF and progressively pinch out 30–50 km west of the
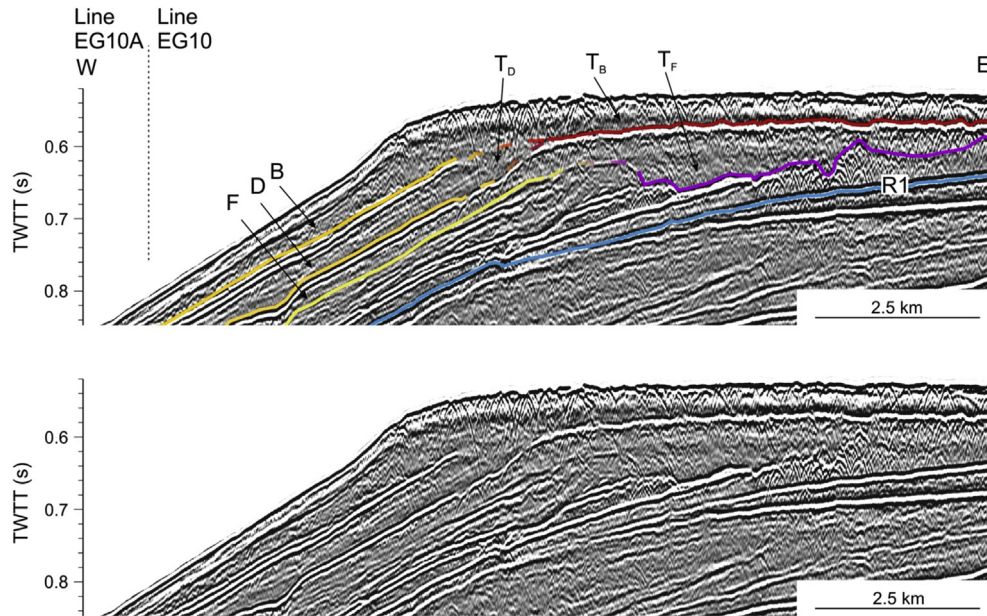
Fig. 5. Top. Interpreted cross-section. Bottom. MCS airgun seismic reflection profile perpendicular to shelf edge (for location see Fig. 2) showing the transition between units on the shelf and slope. The red to purple lines on the shelf correspond to the base of subglacial deformation tills, which grade laterally into GM debris flows (basal reflectors marked in shades of yellow) on the slope. (For interpretation of the references to color in this figure legend, the reader is referred to the web version of this article.)

shelf edge. In these areas, they form a distinct package made of stacked transparent lenses, while in the southernmost part of the Storfjorden TMF, these lenses occur rather isolated within the laminated units and their continuity, particularly for unit B,

might be lost (Fig. 6). Unit α is significantly more discontinuous than the preceding units and is present only in the upper and mid slope in the central and northern area of the Storfjorden TMF.
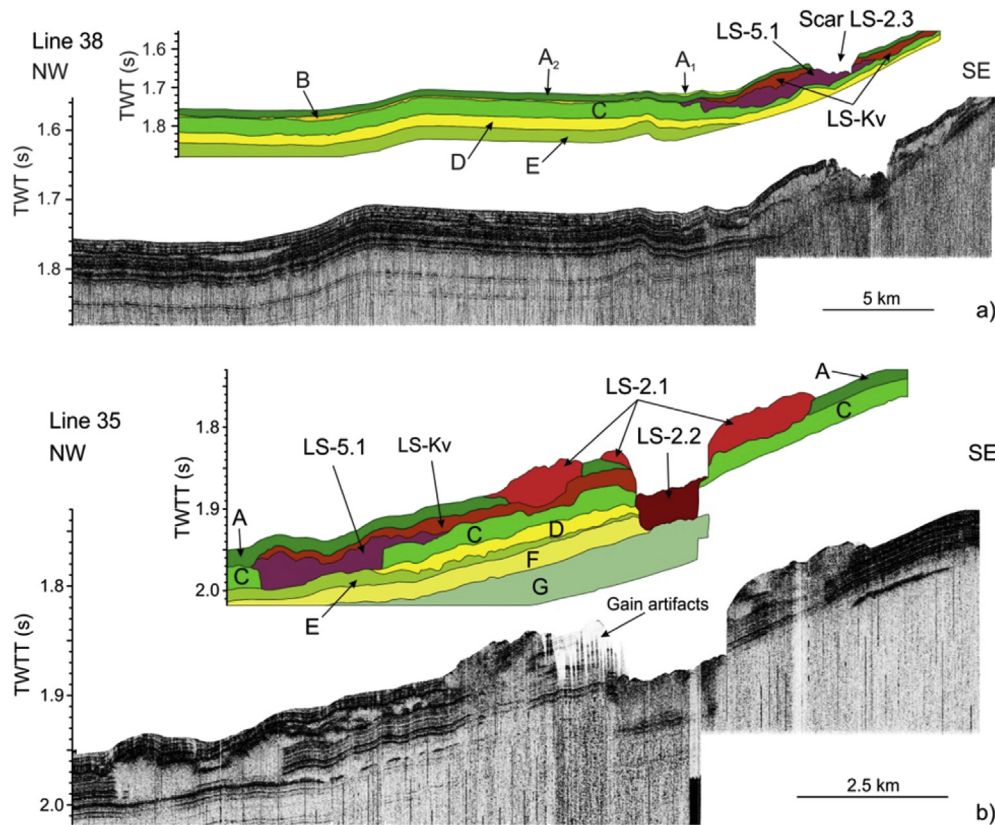

Fig. 6. a) Top interpreted cross-section. Bottom TOPAS sub-bottom profile Line 38 (for location see Fig. 2) illustrating an area with homogeneous thickness of both GDFs (shades of yellow) and IGM laminated (shades of green) units. Unit B is not present in this area. Submarine landslides (red and purple) erode laminated and transparent units. b) Top interpreted cross-section. Bottom TOPAS sub-bottom profile Line 35 (for location see Fig. 2) showing stacked landslides, erosive boundaries and scars associated to landslides. GDFs are shown in shades of yellow, IGM units in shades of green and submarine landslides in shades of red and purple. (For interpretation of the references to color in this figure legend, the reader is referred to the web version of this article.)

4.2. Sedimentology

Cores collected during the SVAIS cruise have sampled units A and B, in addition to the more chaotic units associated with the scarps (for a detailed sedimentological analysis see Lucchi et al. (2012) and Lucchi et al. (2013)). Subunit A_1 consists of heavily bioturbated and crudely layered mud, and structureless IRD-rich silt. Subunit A_2 is composed of finely laminated mud interbedded with sandy layers. Red oxidized beds have also been identified near the base of unit A_2. Unit B consists of a water-poor, high shear strength diamicton. The boundary between units A_1 and A_2 has been dated in between 12 and 10 cal ka BP while the boundary between units A_2 and B has been dated at ~20 cal ka BP (Sagnotti et al., 2011; Lucchi et al., 2012). The transparent/chaotic units that are associated with slope scarps have also been sampled as low shear strength, water-rich diamictons, which physical properties resemble the laminated sediments (~40% water content, shear strength up to 20 kPa) rather than the diamictons in unit B.

4.3. Surface geomorphology of sub-surface features

A number of surface morphologies on the shelf and slope are associated with sub-surface features and the sedimentary units described above, particularly the shallowest sedimentary units. On multibeam bathymetry data the most conspicuous feature on the TMF is a network of gullies on the upper slope. Individual gullies are 200–1000 m wide, 10–15 m deep and 5–50 km long and are mainly located in the north and central part of the Storfjorden TMF. Downslope, these gullies gradually fade out (no gullies are present beyond the 1000 m isobath) and most do not cut back into the shelf. The downslope termination of these gullies often displays lobate convex-upward sedimentary bodies. Evidence for gully-like features is also observed in sub-bottom profiler, SCS and MCS data (Figs. 3 and 4). The gullies observed on bathymetric data can completely or partially cut into unit A (A_1 and A_2), be draped by unit A_1 or be filled by the entire unit A.

Paleo-gullies are wider (2–4 km) and deeper (12–40 m) than the present-day gullies observed on the bathymetric data. The paleo-gullies are also preferentially present in the northern and central part of the Storfjorden TMF and gradually disappear to the south and west. They develop at the top of well-stratified units (C, E and G), which can be completely or partially eroded, but hardly incise into the units made of stacked transparent lenses (B, D and F) (Fig. 4). In turn, transparent units B, D and F fill the paleo-gullies. South of the Kveithola TMF, the drainage network develops from the shelf break into a dendritic canyon system rather than gullies (Fig. 2). The termination of these canyons is not imaged in the available data set.

The confluence between the Storfjorden and Kveithola TMFs is also the area where a series of surface scarps are located (Fig. 6). The length, width and height of these scarps are highly variable ranging from 1.7 to 40 km, 0.5 to 8 km and 10 to 50 m respectively. All scarps are located in between the shelf edge and the 1600 m isobath, but within this depth range there is no preferential depth of occurrence of the observed scarps. The scarps are associated with near-surface or sub-surface transparent to chaotic lenses of sedimentary deposits (transparent acoustic response in TOPAS profiles and chaotic in SCS and MCS profiles) (Fig. 6). These deposits are classified into those that have a surface expression (LS) and those that do not have such an expression (PLS). Twenty-six such bodies (LS and PLS) have been identified in the study area. In sub-bottom profiler data, most of the seismically transparent sedimentary bodies associated with slope scarps are actually composed of clustered transparent lenses. The majority of these bodies have unit C at the bottom and, in most cases, they are devoid of sediment at their top (Table 2, Figs. 6 and 7), implying that those are amongst the most recent events in the sedimentary succession. One of the largest transparent bodies associated with scarps on the TMF is LS-1. The headscarp of LS-1 is made of several coalescent scarps with a total height of up to 80 m. However, typical head/side scarps are 30–40 m high. Several transparent/chaotic bodies are associated with the coalescent scarps of LS-1. The larger of these bodies (LS-1.1) has a minimum area of 1340 km^2 and a mean thickness of 35 m; the total amount of sediment involved in this sedimentary body is ~47 km^3. The three deposits that have no surface expression (PLS-1, PLS-2 and PLS-3; see also Rebesco et al. (2012)) (Fig. 8) have a minimum volume of 45 km^3, 127 km^3 and 18 km^3 respectively (Table 2).

On the outer shelf, the surface expression of seismic units and other sub-surface features on the seafloor is rather scarce. The only exception is a transparent sedimentary lens on the southern side of the outer Storfjorden Trough. In plan view, this sedimentary body displays a drop-like shape (Fig. 7). At their top surface, the various units that subcrop in the near surface of the shelf display linear to curved furrows and sets of larger-scale parallel lineations. The latter typically occur in groups of 5–6 lineations (Fig. 7).

4.4. Seismic units distribution and related thickness

The occurrence and thickness of the "laminated" and "transparent" seismic units is not constant either laterally (along/across slope) or with depth within the sedimentary sequence (older units). In particular, the acoustically laminated seismic units drape the entire slope of the TMF, while the transparent units develop only on the upper and middle slope, especially in the two northernmost lobes of the Storfjorden TMF (Lobes I and II).

In general, the thickness of the laminated units (A, C, E and G) increases southwards and with depth in the sedimentary column (older units). Thickness also decreases downslope showing a more constant pattern than the transparent units, which have high lateral thickness variation (Fig. 9). The uppermost laminated unit, unit A, drapes the entire area imaged by our data set with a mean thickness of 10 ms twtt although thickness increases both south and north to the sides of the TMF. Of these 10 ms twtt, 2–4 ms twtt correspond to subunit A_1. Unit A_1 can be tracked on both the shelf and slope through the shelf break. Unit A's maximum thickness of 39 ms twtt is reached in the inter-TMFs area and on the Kveithola outer shelf where distinct depocenters are found both in the upper and middle slope (Fig. 9a). Unit C has a relatively constant thickness in the northern and central Storfjorden TMF of 20–30 ms twtt. Maximum sediment accumulations of up to 64 ms twtt occur in the southern Storfjorden and northern Kveithola TMFs close to the shelf edge (Fig. 9c). As is the case with unit A, a few depocenters are present in this unit. The main depocenter is located in the upper-middle slope of the inter-TMF area, but secondary depocenters occur in the middle slope of the southern TMF. Units E and G are not sufficiently imaged, but available data suggest that unit E is similar in thickness to unit C and that unit G is the thickest laminated unit above R1 in the TMFs with a mean thickness of 90 ms twtt (Fig. 4).

The transparent units (B, D and F) display highly variable thickness. They form relatively continuous layers in the upper and middle northern and central Storfjorden TMF. They however occur in isolated lenses or even disappear, particularly unit B, in the southern part of the Storfjorden TMF and at the confluence with the Kveithola TMF (Fig. 6). These units also decrease in thickness downslope and they pinch out 30–50 km away from the shelf edge. Unit B is the transparent unit which thickness is better constrained due to penetration issues. It has a spatial distribution displaying the opposite pattern to that of the above and below laminated units, A and C (Fig. 9b). The maximum thickness is around 89 ms twtt close to the central part of the Storfjorden TMF and almost disappears to

Table 2
Landslides characteristics. The mean thickness is calculated from the height of the scar above and below the sea floor. The volume corresponds to the area and height where the scars have been identified *: feature not completely imaged. ?: not visible.

	Bottom unit	Top unit	Area (km^2)	Mean thickness (m)	Volume (km^3)
LS-1.1	pre-R1	D	1338.4	35.0	46.84*
LS-1.2	B	–	11.0	15.6	0.17
LS-2.1	C	–	95.2	26.0	2.48*
LS-2.2	C	–	35.5	30.0	1.06
LS-2.3	B	–	12.7	25.0	0.32
LS-2.4	C	A	8.9	20.2	0.18
LS-3.1	C	–	12.7	21.0	0.27
LS-3.2	C	–	3.7	21.0	0.08
LS-4.1	C	–	13.0	23.0	0.30
LS-4.2	C	–	5.2	26.0	0.14
LS-4.3	A	–	2.6	12.0	0.03
LS-5.1	C	A	86.0	46.0	3.96
LS-5.2	C	A	4.8	11.2	0.05
LS-5.3	A	–	0.8	9.7	0.01
LS-6	A	–	3.8	8.2	0.03
LS-7	C	–	6.7	32.2	0.22
LS-8.1	C	–	2.9	16.4	0.05
LS-8.2	C	–	4.9	17.2	0.08
LS-9	C	–	67.3	11.2	0.75
LS-10	C	–	36.2	12.7	0.46
LS-11.1	?	–	119.9	17.2	2.06
LS-11.2	?	–	52.9	21.0	1.11
LS-Kv	C	A	459.1	8.0	3.67*
PLS-1	pre-R4	post-R3	647.7	70.0	45.34*
PLS-2	pre-R1	E	709.0	180.0	127.62*
PLS-3	pre-R2	R2	240.0	75.0	18.0

the south of the TMF. Close to the shelf edge, a few seismic lines show evidence that the slope transparent units grade into the shelf transparent units (T_B, T_D, T_F), where their thickness varies between 3 and 120 ms twtt (Fig. 5).

There are few areas where unit D has been fully imaged, and therefore the isochore map does not show clear thickness trends. However, we find a more constant thickness across the study area with a mean value of ~25 ms twtt and maximum values up to 40 ms
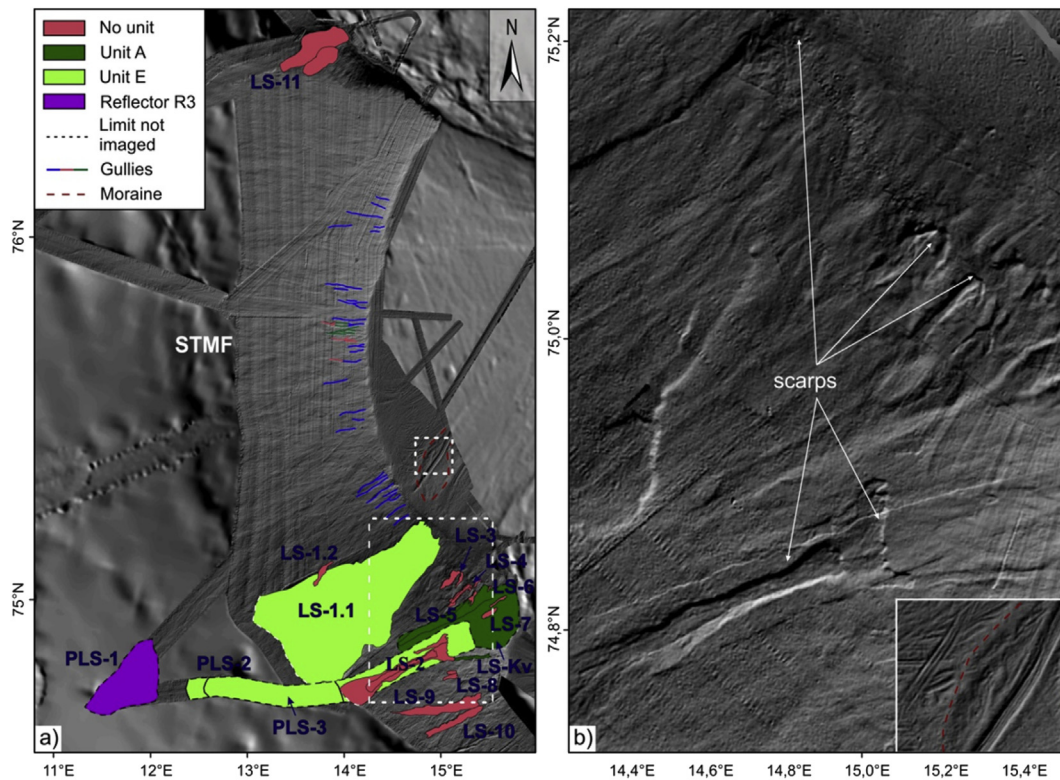

Fig. 7. a) Shaded relief image with landslides and recent gullies identified on the continental slope of the Storfjorden and Kveithola TMFs. The color-coding of landslides identifies the draping unit/reflector of the landslides. Some of the landslides are complex with multiple stages involved in the same event. For detailed characteristics of each landside see Table 2. Gully color identifies the gully relationship with unit A: blue is gully fully filled with unit A; pink-red is gully with partial accumulation of unit A$_2$; green is gully devoid of sediments. Red dashed line marks a morainal body. White dashed squares marks the two close-up views in b). STMF: Storfjorden Trough Mouth Fan; KvTMF: Kveithola Trough Mouth Fan. Note bathymetric artifacts induced by slope parallel ship tracks. b): shaded relief bathymetry showing close-ups of slide scarps at the confluence area between the Storfjorden and Kveithola TMFs, and plough marks on the shelf. (For interpretation of the references to color in this figure legend, the reader is referred to the web version of this article.)
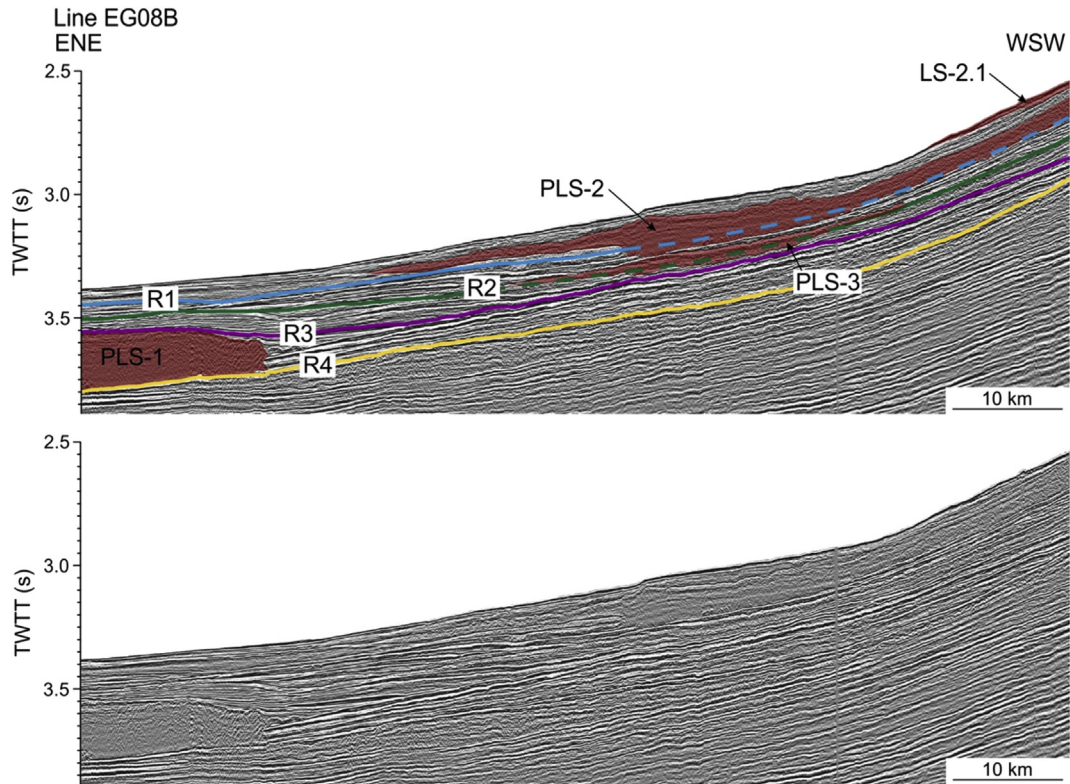
Fig. 8. Top. Interpreted cross-section showing landslides PLS-1, PLS-2, PLS-3 and LS-2.1. Bottom. Airgun seismic reflection profile (for location see Fig. 2). Regional reflectors R1 to R4 are highlighted (after Rebesco et al. (2012)). Dashed lines tentatively show the position of reflectors prior to the occurrence of landslides PLS-2 and PLS-3.

twtt in the upper central fan area (Figs. 4 and 6). Imaging of unit F in SCS and MCS data is not complete enough to produce isochore maps, however available data suggest that above R1 the three transparent units identified display an increasing thickness with depth, being the uppermost unit (unit B) thinner.

The isochore map between the regional reflector R1 and the sea floor (Fig. 9d) computed from the interpretation of SCS and MCS data shows that the main depocenter is located in the upper/middle slope and, particularly, close to the shelf edge. The mean values in this area are 220 ms twtt, while maximum values of 340 ms twtt occur in the central part of the Storfjorden and Kveithola TMFs close to the shelf break. The thickness of the TMF above R1 quickly decreases towards the north and west displaying a pattern similar to the transparent units, which likely seem to control overall thickness above R1.

5. Discussion

5.1. Interpretation of acoustic facies and seismic units

Using the cores collected in the Storfjorden trough and TMF, the uppermost seismo-stratigraphic units can be correlated to sedimentary lithofacies. The uppermost subunit A_1 is characterized by a poorly laminated and bioturbated mud in sedimentary cores and it is interpreted as Holocene interglacial sediments (Lucchi et al., 2012, 2013). The high-amplitude well laminated A_2 subunit is characterized by finely laminated mud interbedded with sandy layers and it is interpreted to result from meltwater sediment-laden plumes induced by lift-off and rapid retreat of the ice sheet during deglaciation of the margin. Because the acoustic character of unit A_2 is very similar to that of units C, E and G, we interpret those to be formed under similar environmental conditions and to

correspond also to meltwater plumites. The top of the transparent unit B has been sampled in core SV-02 and is characterized by highly consolidated diamicton. Unit B has been interpreted as a series of amalgamated glacigenic debris flows (GDFs), which were deposited during glacial maxima (Pedrosa et al., 2011). The GDFs originated from glacigenic sediments dumped over the shelf edge as this sediment was being pushed by the ice streams (see also Laberg and Vorren, 1995). GDFs of unit B have low water content (~23%) and high shear strength (~40 kPa) compared with the sediments of unit A that have water contents ~45% and shear strengths ranging between 2 and 12 kPa. The hemipelagic sediments of unit A_1 are found both on the slope and continental shelf, while plumites of unit A_2 on the slope gradually pinch out until complete disappearance close to the shelf edge. Conversely, GDFs on the slope grade into transparent units on the continental shelf that have not been sampled in this work. These transparent units on the shelf have a more tabular character and a distinct morphological expression with respect to the transparent units of the slope. Amongst the features associated with these shelf transparent units are linear to curved furrows and sets of larger-scale parallel lineations (Fig. 7). From these characteristics, we interpret the transparent units on the continental shelf as a series of ice front and basal deformation tills. On the shelf, we identified three till units (T_B, T_D, T_F). These tills grade laterally, across the shelf edge, into units B, D and F respectively (Fig. 5). Erosion during ice stream readvance over the shelf may partially or completely erode older till units. An additional T_α unit, much thinner, located just below unit A_1, has been mapped along a few lines on the Storfjorden shelf but could not be confidently correlated through the shelf edge with unit α.

Cores SV-04 and SV-05 (Fig. 2) sampled the transparent bodies on the slope associated with scarps and frequent lateral erosive
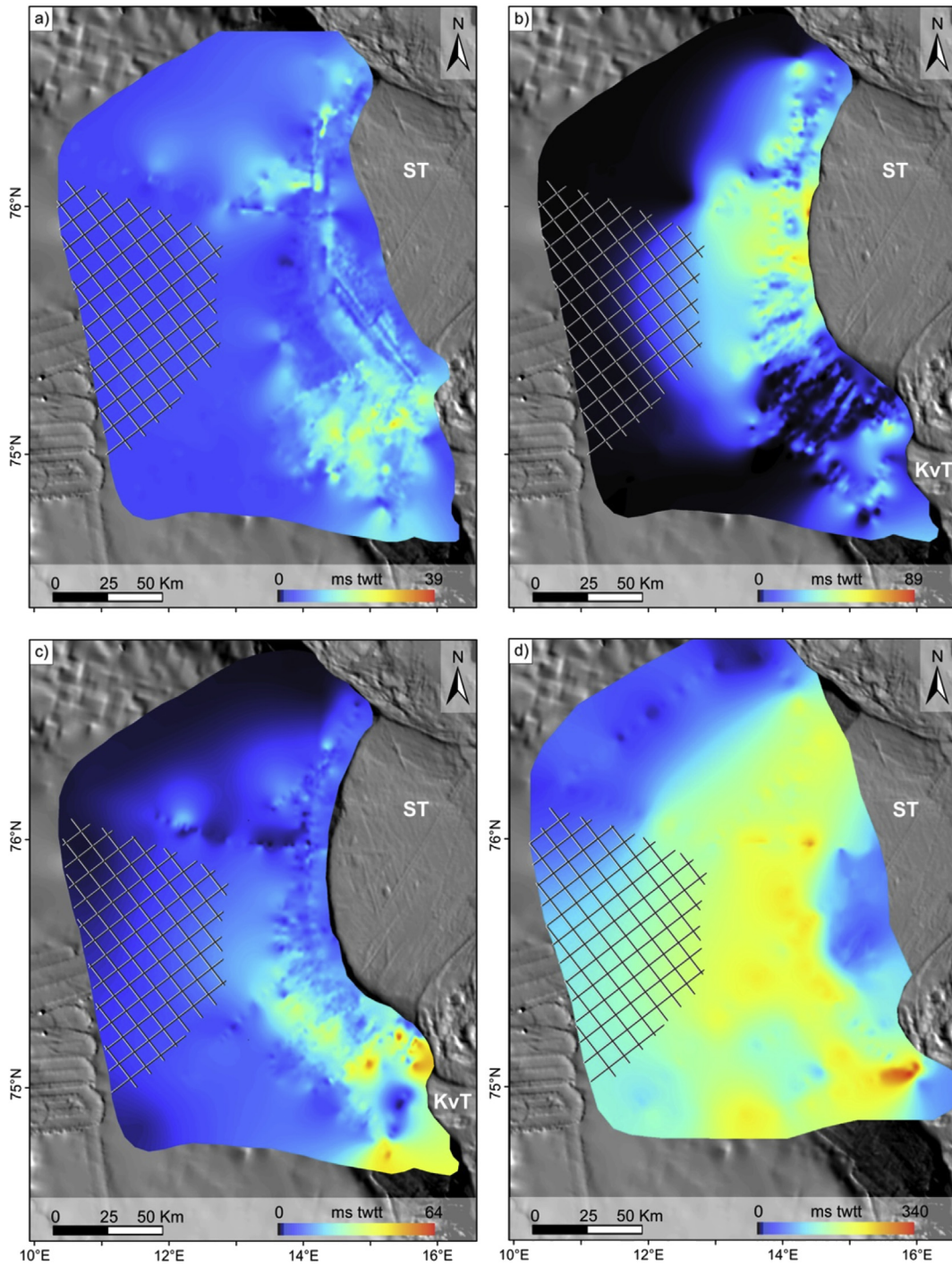
Fig. 9. Isochore maps showing the thickness (in ms twtt) of a) unit A, b) unit B, c) unit C and d) total thickness above the R1 regional reflector. Gray mesh depicts area with no seismic coverage and interpolated values. Grid cell size is 80 m. ST: Storfjorden Trough; KvT: Kveithola Trough. Note that color bars do not have the same scale. (For interpretation of the references to color in this figure legend, the reader is referred to the web version of this article.)

boundaries cutting into units A and B. These sediments are diamictons characterized by high water content and relatively low bulk density when compared to the GDF of unit B. These diamictons have been identified as debris flows associated with submarine landslides. They respond to the dynamics of the slope rather than to processes originating in the continental shelf, as in the case of GDFs. Most of the landslides are located at the confluence of the Storfjorden and Kveithola TMFs and have an acoustically laminated unit at their base and either are devoid of sediments or have another

laminated unit at their top.

5.2. Glacial dynamics of the Storfjorden paleo-ice stream

The relative high-density of high-resolution seismic reflection profiles available in the area provides a unique opportunity to understand the detailed history of sediment delivery from the Storfjorden and Kveithola paleo-ice streams to the respective TMFs. Such sediment delivery was highly variable in space and time

(Fig. 9). Subunit A$_2$, a deglacial unit largely corresponding to meltwater plumites, displays a thicker sediment package to the south of the Storfjorden TMF (lobe III; Fig. 6) and on the Kveithola TMF. On the other hand, unit B corresponding to GDFs deposited during the Last Glacial Maximum shows thicker sediment accumulations in the north and central part of the Storfjorden TMF. The isochore map of unit B displays a radial pattern spreading from the shelf edge, which results from the presence of GDF downslope elongated lenses. These GDF lenses are comparatively thicker than the other lenses within the unit in the northern and central TMF or they occur as isolated lenses within the bounding laminated units in the southern TMF. Such distribution indicates that individual sedimentary bodies within the transparent unit originate from the shelf break and are transported downslope to the mid-slope (Fig. 9b). Seismic records where previous units can be imaged, suggest that deglacial and glacial maximum related units display a similar distribution pattern to units A$_2$ and B respectively. The thicker GDF units in the northern fan area significantly contributed to shelf edge progradation from R1 time to present. In lobe I this progradation is around 6 km while in the southernmost lobe III it is just 2.2 km. The difference in progradation and better developed GDF units supports the idea suggested by Pedrosa et al. (2011) that, to the north, the Strofjorden ice stream had thicker and perhaps faster ice. Alternatively, the northern sub-ice stream I could have transported a higher sediment load from drainage of a distal and larger ice source. Two shallow banks on the outer shelf of lobe I (60–70 m above the surrounding shelf) (Fig. 1) could have provided an anchoring area for the ice stream in the northern sector favoring the stabilization of the ice. In turn, lobe III and the Kveithola Trough could have slower and thinner ice within the ice stream that was fed from a smaller catchment area in Spitsbergenbanken, therefore preventing more significant erosion and supply of sediment to the shelf edge in the form of GDFs.

The thinner "laminated units" in the northern and central lobes suggest also that the last deglaciation of Storfjorden was relatively rapid. The outer Storfjorden Trough is devoid of laminated units such as those found in the TMF, however the Kveithola Trough hosts a 15 m thick glacimarine sequence inferred to have been deposited during the last deglaciation (Rebesco et al., 2011; Bjarnadóttir et al., 2013). This suggests that there was significantly higher sediment availability in the Kveithola system during the deglaciation, likely because a marine-based ice cap remained closer to or sitting on the shallow banks surrounding the Kveithola Trough. Plumites were possibly funneled through the narrow Kveithola Trough and redistributed along the Kveithola TMF and may possibly have been drifted to the southern Storfjorden TMF by the WSC.

Meltwater discharge from underneath an ice sheet grounded at the shelf edge may have also contributed to gully formation (Noormets et al., 2009; Pedrosa et al., 2011; Gales et al., 2013; Lucchi et al., 2013). The fact that some gullies are often draped by unit A$_1$ (Holocene sediments) and in some instances they even have some A$_2$ infill (Fig. 4), suggest that they were formed synchronous with plumite deposition. Preferential occurrence of the gullies in the northern and central part of the Storfjorden TMF suggests that the meltwater discharge was more intense and again points to a faster ice-stream retreat in the northern part of the trough.

5.3. Storfjorden TMF chronostratigraphic framework

Eight units have been mapped above regional reflector R1. These units involve the same time interval as units B to G of Sættem et al. (1992, 1994), units III to VIII of Laberg and Vorren (1996a) in the Bear Island TMF, and units C to G of Laberg and Vorren (1996b) in Storfjorden (Fig. 10). They all belong to the megasequence GIII of

Hjelstuen et al. (1996) (Table 3). Nevertheless, there is significant variability in the ages proposed for the different units largely owing to the various dating methodologies. Laberg and Vorren (1996b) used the land record (Mangerud and Svendsen, 1992) as well as correlation to the oxygen isotope curve of Williams et al. (1988) to constrain the age of their units E, F and G (Fig. 10). These units respectively match the Marine Isotopic Stages (MIS) 2, 4 and 6 (Lisiecki and Raymo, 2005; Hao et al., 2012). Mangerud et al. (1998) also suggested that 4 major ice advances occurred over the Western Svalbard shelf (Fig. 10). Their glaciations G, E and A respectively correspond to our glacial units B, D and F.

In this study, we propose an age model for the observed units in the Storfjorden and Kveithola TMFs that takes into account ages reported in the area as well as dating of our sediment cores (Laberg and Vorren, 1996b; Mangerud et al., 1998; Sagnotti et al., 2011; Lucchi et al., 2013). The basis for our age model are the AMS ^{14}C dating of the boundary between units A and B on cores SV-02 and SV-05, representing the transition from the LGM to deglaciation, at 18–20 ka BP. These dates are in agreement with those of Andersen et al. (1996) and Mangerud et al. (1998) indicating that, the ice sheet in the Svalbard-Barents Sea retreated from the outer shelf earlier than 17.7 ka BP. Jessen et al. (2010) and Rasmussen et al. (2007) also point that the Storfjorden ice stream had retreated at least 35 km from the shelf edge at 19.2 ka BP. These dates are also in agreement with the scenario outlined by Bjarnadóttir et al. (2013) in the Kveithola Trough, documenting the onset of deglaciation between 21.5 and 19 cal ka. The Kveithola Trough is much smaller and slightly shallower than Storfjorden and the ice source, in Spitsbergenbanken, is also closer to the trough, which resulted in slightly lower retreat rates than in Stofjorden (Bjarnadóttir et al. (2013); Fig. 1). Because the passage from the acoustically transparent unit B to the laminated unit A in SVAIS cores involves the transition from the LGM to the deglaciation phase, we infer that all passages from acoustically transparent to laminated units represent the transition from previous glacial maxima to the deglaciation phases. In this study we combine the 57 δ^{18}O worldwide composite record of Lisiecki and Raymo (2005) and Hao et al. (2012) with the δ^{18}O record from core M23385 (Dokken and Hald, 1996), located around 135 km off the Storfjorden shelf edge at 2498 m water depth (Figs. 1 and 10), to constrain the ages of units B, C, D, E, F and G. Since the deglacial and interglacial sediments inside previous laminated units cannot be properly separated in the seismic record, we choose to divide the sequence into Glacial Maximum (GM) and Inter-Glacial Maximum (IGM) periods, the latter corresponding to the deglaciation/interglacial/onset-of-glaciation interval, rather than the classical glacial/interglacial periods. Onset of the last deglacial sedimentation in the Storfjorden TMF, according to the SVAIS cores, starts 5 kyrs earlier than the transition from MIS 2 to 1 Fig. 10). For preceding glacial maxima, we therefore tentatively estimate the onset of deglacial sedimentation 5 kyrs earlier than transition from a "cold" to a "warm" MIS (Fig. 10, Table 3).

The seismic record indicates the existence of a minor GDFs event (unit α) within unit A$_2$. Unit α possibly correlates with the deformation till Tα on the northern shelf record (Fig. 5). The existence of a massive IRD layer within already IRD-rich bioturbated sediments has been associated with Heinrich layer H1 (16.8 cal ka BP) (Lucchi et al., 2013). From its stratigraphic position unit α most likely correlates also to Heinrich layer H1, indicating a short-lived re-advance of ice sheets on the shelf south of Svalbard similar to the one that occurred in Kveithola between 16 and 15.5 cal ka (Bjarnadóttir et al., 2013).

With regards to the onset of glacial maximum sedimentation (GDFs), we have no absolute ages for the time when ice streams reached the shelf edge in the Storfjorden and Kveithola Troughs at
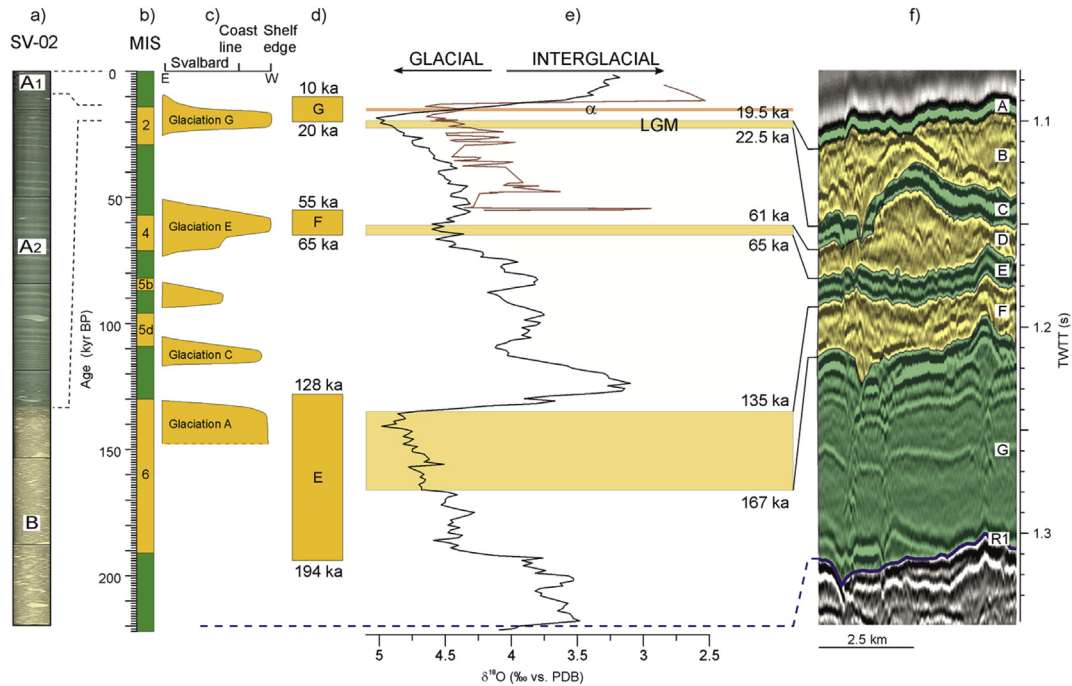
Fig. 10. Proposed age model of the different GM (shades of yellow) and IGM (shades of green) units. a) Core SV-02, b) Marine Isotopic Stages (Lisiecki and Raymo, 2005), c) advance over the shelf of the western Svalbard ice sheets (Mangerud et al., 1998), d) age estimates of glacigenic units based on correlation to the Svalbard land record (Laberg and Vorren, 1996b), e) proposed ages in this study, black line: δ18 oxygen isotope curve for a world composite of 57 cores (Lisiecki and Raymo, 2005; Hao et al., 2012), red line δ18 oxygen isotope curve of core M23385 (see Fig. 1), f) seismic stripe from line SVAIS06 of full studied period. (For interpretation of the references to color in this figure legend, the reader is referred to the web version of this article.)

the beginning of the Late Weichselian glacial maximum. Recent studies indicate that the ice sheet reached the shelf break west of Svalbard at 24 ka BP (Jessen et al., 2010). South of Storfjorden, in Bjørnøyrenna, ice streams reached the shelf break around 22 ka BP (Landvik et al., 1998; Svendsen et al., 2004). Available data therefore suggest that unit B, corresponding to the Weichselian glacial maximum, was deposited from 22.5 ka BP. Therefore, the ice stream grounded at the shelf edge ~6 kyrs later than the start date of MIS 2. Based on this criterion, we estimate the onset of previous GM sedimentation (GDF) 6 kyrs later than the transition from a "warm"

to a "cold" MIS (Fig. 10). In the case of unit F, onset of GDF sedimentation is made proportionally to the length of the glacial period (24 kyrs).

According to the aforementioned criteria, we propose that the GM units D and F are 61–65 ka BP and 135–167 ka BP, respectively (Table 3). The base of unit G corresponds to reflector R1. The ages proposed for reflector R1 are 700 ka BP (Vorren et al., 2011), 440 ka BP (Sættem et al., 1992, 1994; Faleide et al., 1996; Hjelstuen et al., 1996) and 220 ka BP (Butt et al., 2000; Knies et al., 2009; Rebesco et al., 2014). Because we find only three GM units above reflector

Table 3
Correlation of seismic stratigraphic units in this work with those of previous studies in the western Barents Sea continental margin. See text for further discussion.

Western Barents sea	Bear Island TMF			Storfjorden TMF		This work			
Faleide et al. (1996) Butt et al. (2000)	Sættem et al. (1992, 1994)		Laberg and Vorren (1996)	Hjelstuen et al. (1996)	Laberg and Vorren (1996b)	This work			
	Unit	Age (ka)	Unit	Age (ka)		Unit	Age (ka)	Unit	Age (ka)	Mean compacted sed. rates (m/kyr)[b]	Mean decompacted sed. rates (kg m−2 yr−1)[b]

Western Barents sea (Faleide/Butt)	Sættem Unit	Sættem Age	Laberg Unit	Laberg Age	Hjelstuen	Laberg b Unit	Laberg b Age	This work Unit	This work Age (ka)	Mean compacted sed. rates (m/kyr)[b]	Mean decompacted sed. rates (kg m−2 yr−1)[b]
	G	<30						A_1	13–0	**0.1**	
								α	~16.8[a]	**~5**	
			VIII	24–12				A_2	19.5–13	**0.4**	**0.6**[d]
	F					G	20–10	B	22.5–19.5	6.9–**6.9**–7.0	17.6–**17.7**–18.1 (46.9)[c]
	E	130–?						C	61–22.5	**0.3**	**0.8**
	D_2	<200–130	VI	194–128		F	65–55	D	65–61	5.2–**5.4**–5.6	15.1–**15.7**–16.3 (35.1)[c]
								E	135–65	**0.1**	**0.3**
	D_1	<330	V	313–258		E	194–128	F	167–135	0.7–**0.7**–0.8	2.0–**2.1**–2.2 (7.4)[c]
	C		IV	386–359							
R1 <440 ka**, 200 ka#	B	<440	III	486–430	GIII (440 ka)			G	220–167	1.3–**1.4**–1.5	3.1–**3.5**–3.7

**Signifies that the age reported is from Faleide et al. (1996) while the #signifies that the age is from Butt et al. (2000).
[a] Unit α is embedded within A2.
[b] Minimum–**most probable**–maximum sedimentation rates respectively computed with a constant 1.5 km/s velocity, a p-wave velocity increasing with a 1.48 + 1.5z function (consistent with the overall velocity gradient for the upper 250 m in ODP Site 986) and a velocity increasing with a 1.5 + 2.13z function (consistent with the velocity gradient in the SVAIS piston cores). Minimum and maximum values are only plotted if they differed by one significant decimal with respect to the mean value.
[c] Highest decompacted sediment rates during Glacial Maxima computed with a p-wave velocity increasing with a 1.48 + 1.5z function.
[d] Refers to the entire A2–A1 stratigraphic interval.

R1 in the Storfjorden TMF area, we favor the 220 ka BP age, in agreement with Butt et al. (2000), Knies et al. (2009) and Rebesco et al. (2014).

Based on the proposed age model for GM units, the mean decompacted sedimentation rates are 2–18 kg m^{-2} yr^{-1} during glacial maxima (Table 3). Where the thickest sediment accumulations occur, the sedimentation rates during GM may reach values of 47 kg m^{-2} yr^{-1} (24 m/kyr for non-decompacted sedimentation rates). The mean sedimentation rates in between GM are very similar and one to two orders of magnitude lower than those of glacial maxima (Table 3). It is possible, as shown by Lucchi et al. (2013), that most sediment in IGM units accumulated in the short deglaciation phases. In this regard, the sedimentation pattern during GM periods is much more punctuated and considering individual GDF lenses may lead to sporadic but much higher instantaneous sedimentation rates. It is clear from these data that the buildup of the Storfjorden TMF, and possibly of all major TMFs, occurs in short pulses during GM and, to a lesser extent during deglaciation. The somewhat lower sedimentation rates in the GM unit F, despite the potentially longer duration of glaciation may be explained from the dynamic behavior of the ice sheet, which could possibly be cold-based with less sediment transported subglacially (Cuffey et al., 2000; Winsborrow et al., 2010). In the case of the IGM unit G, the high sedimentation rates (3.5 kg m^{-2} yr^{-1}) compared to units A, C and E (0.3–0.8 kg m^{-2} yr^{-1}) may point to an older age of reflector R1. An age of 440 ka as suggested by Faleide et al. (1996), Hjelstuen et al. (1996); and Sættem et al. (1992, 1994), would yield mean sedimentation rates of 0.6 kg m^{-2} yr^{-1}, similar to the other IGM units. This would imply however, that 2 GM phases (units D and C of Laberg and Vorren, 1996b) would have left no record in the TMF.

5.4. Control of TMF architecture on submarine slope failure and timing

It is known that high sedimentation rates, particularly in low permeability sediments, may induce excess pore pressure and subsequent slope instability (Dimakis et al., 2000; Lee, 2009; Micallef et al., 2009). This is often recorded as submarine landslides on continental margins. Given the high sedimentation rates that the Storfjorden TMF experienced during glacial maximum periods, it is highly likely that excess pore pressure could cause the observed landslides (Fig. 7). However, we find that whenever the landslides have a younger unit on top, this unit is either an IGM unit (Fig. 6) or a fully preserved GM unit, suggesting that the landslides occurred during the deglaciation or subsequent interglacial period (Fig. 11a). Here we consider that landslides without cover (identifiable on TOPAS profiles) occurred after deposition of the deglaciation unit A$_2$, and sometime during the sedimentation of the present interglacial unit A$_1$.

Comparing the sedimentation rates of the different units with the volume and number of submarine landslides (Fig. 11b) shows that the number of landslides was highest after deposition of unit B, which also shows the highest sedimentation rates. However, there is very likely a bias in the number of landslides that can be observed in the most recent units, as those can be mapped from higher resolution data. Most (~75%) of the landslides have an IGM unit as the detachment layer suggesting that loading by GDFs built-up pore pressure in these water-rich sediments (see also Laberg et al. (2002) and Bryn et al. (2005) for similar slope failure scenarios in formerly glaciated margins). Nevertheless, the largest landslides occurred after sedimentation of the GM units that showed lower sedimentation rates. PLS-2, the largest landslide in the study area (Table 2, Fig. 8) is located below unit E and affected units F (GM) and G (IGM), the latter being the thickest IGM unit

above reflector R1. Most landslides are located in the inter-TMF area between Storfjorden and Kveithola where the IGM units are also thicker. From this, we infer that the volume of the landslides (and perhaps the number) is not controlled by the sedimentation rates of the GM units, but rather by the sedimentation rates and overall accumulation of sediments deposited during the previous IGM period (Fig. 11c). This leads to several pre-conditioning (pore-pressure build-up) scenarios depending on multiple combinations of the deposited thickness of IGM sediments and subsequent accumulation rates of GDF units during GM. The timing of the landslides indicates that sedimentation of this "unfavorable" stratigraphy was, however, not enough to trigger the landslides, as we observe that failure occurred post-deposition of the GDF units.

Numerous faults are present in and nearby the Storfjorden Trough (Fig. 1). The Hornsund fault zone is a major NW-SE structural lineament with clear bathymetric expression located 70 km from the shelf edge (Fig. 1) (Faleide et al., 2008). Other tectonic structures in southern Svalbard continue offshore with a clear bathymetric expression. Hampel et al. (2009) modeled fault response during growth and decay of an ice sheet. Their results indicate that ice unloading increases the number and magnitude of earthquakes compared to the loading phase. These periods of increased seismic activity last a few thousand years until activity returns to the normal situation. During the maximum seismogenic phase earthquakes with a moment magnitude M_w ~8 were possible in the NW Barents Sea. The sequence of events leading to the observed instabilities would therefore involve: 1) overpressure build-up in the high water content IGM laminated units during rapid deposition of thick GDF units, preconditioning the margin to failure and 2) triggering by earthquakes induced by isostatic rebound during, or shortly after, the ice retreat. Recurrent, large-scale, climatically controlled slope failures also exists in the Bjørnøya and Isfjorden TMFs, south and north of the study area (Marr et al., 2002; Hjelstuen et al., 2007).

5.5. A cyclic model for TMF evolution

Alternation of GDF units and meltwater plumite units provides the more manifest evidence for a cyclic pattern in sedimentary processes during development of TMFs. However, there is a complex series of sedimentary and erosive processes that act at different periods within a glacial/interglacial cycle to deliver a series of deposits and to produce several landforms (see also Laberg and Vorren, 1996a, 1996b; Taylor et al., 2002; Ó Cofaigh et al., 2003; Lucchi et al., 2013). In this study we suggest a four-stage model for the evolution of Arctic TMFs (Fig. 12), and particularly for the Storfjorden TMF. The model considers the shape and location of the surface and subsurface erosive and depositional features in a spatial frame in combination with the sedimentary record. The location of canyons, gullies, submarine landslides and the GDFs lenses, or even the location within the TMF of all these features contribute to this understanding. These stages are:

a) Interglacial stage: During the present (and previous interglacials) hemipelagic and contour-current influenced sedimentation predominate (Fig. 12a). Based on their stratigraphic position in our seismic records, gully formation in the Storfjorden and Kveithola TMFs cannot be ascribed to only one process or one particular stage. They form by interplay of various processes that act at different stages of TMF evolution. The process and timing of gully formation both in the Arctic and Antarctic have been long discussed (Vorren et al., 1989; Laberg and Vorren, 1995, 1996b; Noormets et al., 2009; Pedrosa et al., 2011; Gales et al., 2013; Lucchi et al., 2013). Because these gullies are most
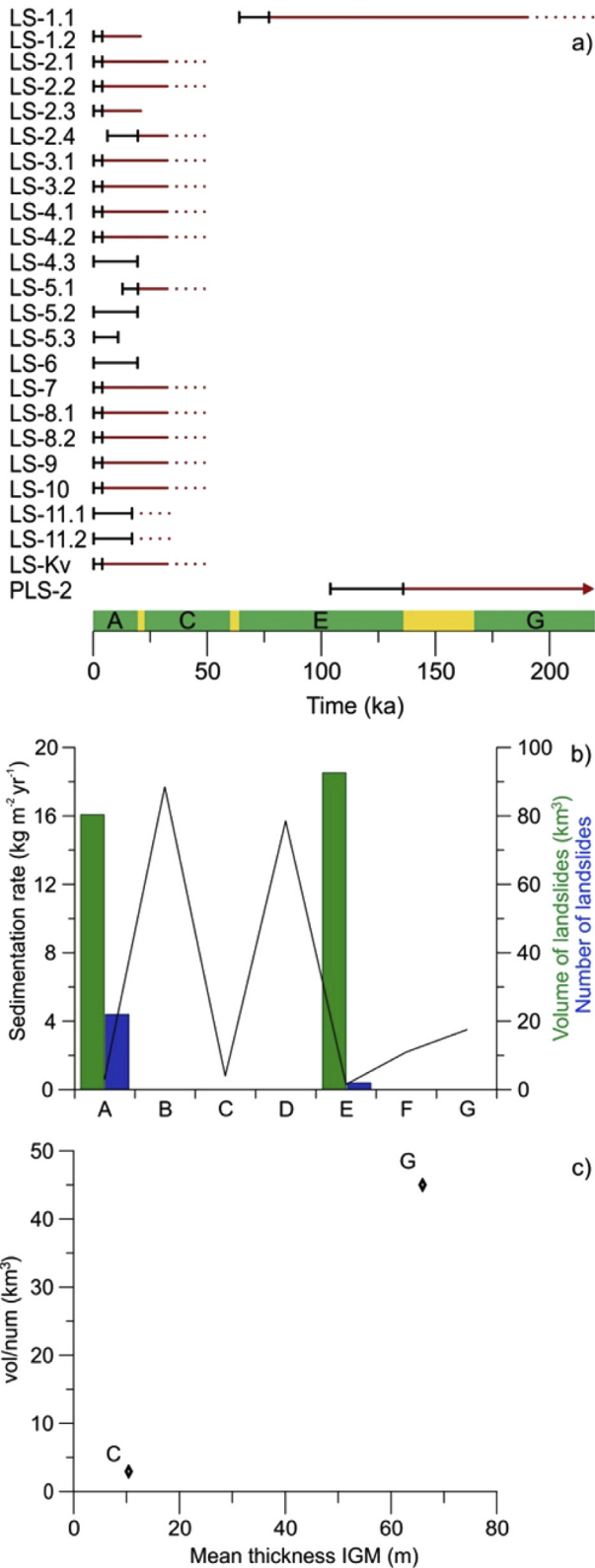
Fig. 11. a) Inferred landslide ages (black line) and age of sedimentary section removed by each landslide (red). b) Mean decompacted sedimentation rates of the different units versus volume and number of landslides for each period. c) Mean thickness of Inter-Glacial Maximum units deposited in the previous interglacial versus landslide unit volume (i.e., landslides that occurred during deposition of unit A are plotted with respect to the thickness of the previous IGM unit, which is unit C). Thicknesses have been calculated using a depth variable sound speed according to the relationship $v_p = 1.48 + 1.5z$ km/s. Note that only landslides above reflector R1 are included. (For

often draped by unit A_1 (Fig. 4), we mainly ascribe them to stage c). However, some gullies are completely devoid of sediment (Fig. 4) implying recent erosion. We hypothesize that some gullies are maintained by dense shelf water cascading (Martin and Cavalieri, 1989; Quadfasel et al., 1988; Schauer and Fahrbach, 1999).

b) <u>Glaciation and Glacial maximum stage</u>: Onset of glaciation is marked by the advance of the ice streams from inland or the inner shelf seawards and IRD distribution due to iceberg calving (Dowdeswell and Elverhøi, 2002). During glacial maxima, ice sheets reach the shelf edge, and the grounding zone sediments together with deforming subglacial till from beneath the ice stream is remobilized as GDFs, due to ice pushing and slope instability (Laberg and Vorren, 1995, 2000; Dowdeswell et al., 1998; King et al., 1998; Ó Cofaigh et al., 2002; Hillenbrand et al., 2005) (Fig. 12b).

c) <u>Deglaciation stage</u>: Rapid deglaciation induces the deposition of plumites along the ice-free shelf and slope. These plumites are the result of subglacial meltwater discharge during rapid ice sheet retreat (Hesse et al., 1997), although meltwater plumes may also occur during the entire life-span of the ice sheet (i.e. Ó Cofaigh et al., 2013). According to dates obtained from the cores in the Storfjorden TMF it is likely, however, that intense plumite deposition took place during the early phase of ice sheet retreat (Lucchi et al., 2013). The rapid decay of the ice sheet was also responsible for the release of large volumes of ice rafted debris throughout the shelf and slope (Fig. 12c and d). Plumite deposition during the deglaciation was accompanied by extensive gully development. Most of the gullies identified developed in between two adjacent GDFs lobes and eroded little into these latter deposits. Erosion or deposition of plumite deposits by subsequent meltwater high-density underflows was determined by the density and velocity of these flows.

d) <u>Slope failure stage</u>: Shortly after deglaciation, unloading of the shelf from the ice mass causes isostatic rebound and associated earthquakes. Ground shaking in already overpressured plumites triggers abundant submarine landslides (Fig. 12d). The location and extent of landslides is related to the thickness of plumite sediments of the previous IGM unit. The debris flows deposits that these landslides produce are completely different in terms of genetic mechanisms, physical properties and timing, than GDFs.

6. Conclusions

Interpretation of an extensive seismic, bathymetric and sedimentological dataset has allowed the detailed, recent (younger than 220 kyrs) sedimentary architecture of two Arctic TMFs, the Storfjorden and Kveithola TMFs, to be characterized.

The late Quaternary (<220 ka) TMFs are made of eight units mostly alternating between glacigenic debris flows (GDF) delivered by ice streams grounded at the shelf edge during glacial maxima, and laminated plumite sequences deposited during the early deglaciation phase. Units of stacked GDFs are mainly present in the northern and central part of the Storfjorden TMF where they are thicker and pinch out towards the lower slope. They also grade into what are probably subglacial deformation tills on the shelf. Deglacial plumite sedimentation is spatially widespread over the TMF, but thicker sequences occur at the confluence of the Storfjorden and Kveithola TMFs. Plumite and interglacial hemipelagic
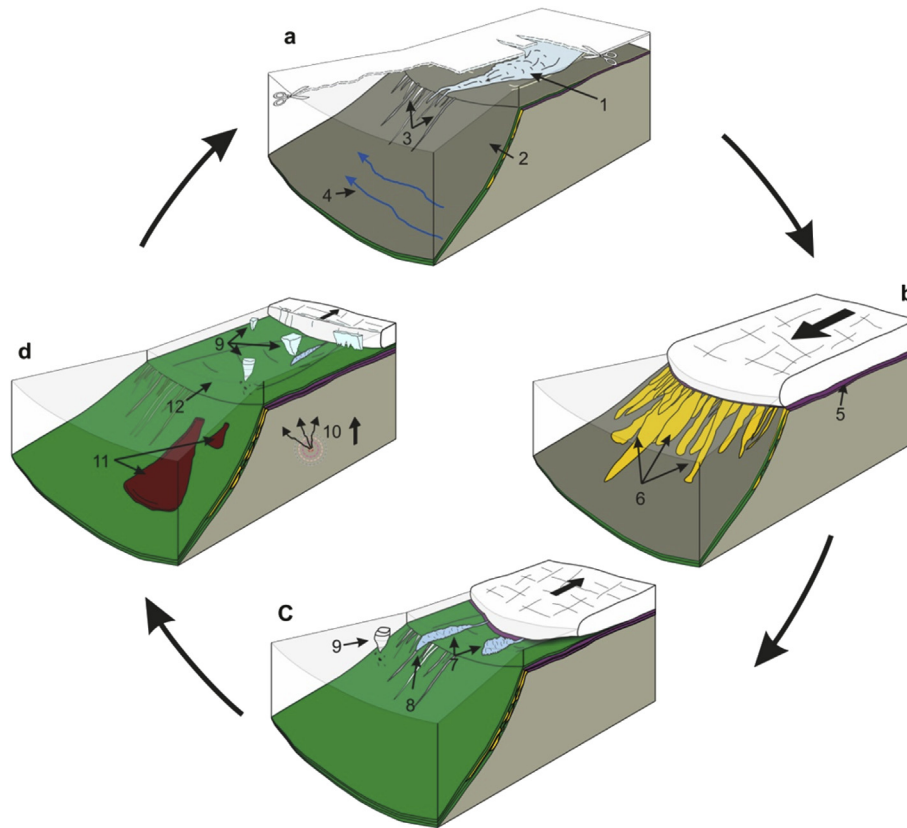
interpretation of the references to color in this figure legend, the reader is referred to the web version of this article.)

Fig. 12. Conceptual model of TMF evolution during a full glacial/interglacial cycle. a: Interglacial stage with hemipelagic sedimentation. During winter, dense shelf water flows due to sea ice formation and brine release maintain free of sediment some of the upper and middle slope gullies excavated during the deglaciation. b: Glaciation and Glacial Maxima, the material transported by ice streams is dumped over the shelf edge as debris flows which can erode the underlying sediments. c: Deglaciation: the turbid meltwater plumes leave a bed of plumites/turbidite sediments covering the shelf and TMF area, while the most energetic flows excavate gullies on the upper slope. The thickness of this unit increases towards the south. d: Submarine landslides triggered by earthquakes from isostatic rebound induced by ice sheet retreat. (1) hyperpycnical flow; (2) hemipelagic (interglacial) sediments; (3) gullies; (4) contour currents, (5) subglacial (diamicton) till; (6) debris flows; (7) meltwater plumes; (8) gully erosion and plumites/turbidite sedimentation; (9) iceberg rafting; (10) earthquake; (11) landslides; (12) glacial trough. In b) to d) sea-ice is not shown for a better visualization of the slope processes.

sediments may partially fill gullies on the upper slope, but some gullies are devoid of sediment fill. We interpret that those gullies form by dense melt-water plumes and, in some instances, may remain active and maintained by cascading of dense shelf-waters.

We suggest a sedimentary model for Arctic TMFs with four major stages involving distinct deposits and sedimentary features. These include a) an interglacial stage dominated by hemipelagic sedimentation and maintenance of gullies carved during the previous deglaciation; b) a Glaciation and Glacial Maximum stage dominated by GDF deposition; c) a deglaciation stage characterized by the rapid accumulation of meltwater plumites and gully erosion, and d) a submarine landslide stage. Within the climate cycle, TMFs mainly record stages b and c, which are likely the shortest periods within a climate cycle. This indicates that sedimentation in TMFs is mainly punctuated rather than continuous through time.

Based on dates from sediment cores and correlation to adjacent areas and previous records, an age model for the identified units is proposed. The age of the GDFs corresponding to the last shelf edge glaciation periods is tentatively estimated at 19.5–22.5 ka (unit B), 61–65 ka (unit D) and 135–167 ka (unit F). The number of GDF units above regional reflector R1 (three) is in agreement with a 220 ka age for this reflector. Ensuing mean decompacted sedimentation rates for glacigenic units are 17.7 kg m^{-2} yr^{-1} for unit B, 15.7 kg m^{-2} yr^{-1} for unit D and 2.2 kg m^{-2} yr^{-1} for unit F, one to two orders of magnitude larger than those of combined deglacial–interglacial sedimentation.

Several submarine landslides have been identified on the surface and sub-subsurface of the TMFs. We find that the majority of landslides occurred during deglaciation or early in the interglacial cycles and they are most often rooted in the previous deglacial/interglacial. From this, we infer that the mechanisms inducing slope failure involve a combination of factors: overpressure and earthquakes due to post-glacial isostatic rebound. An "unfavorable" stratigraphy arises from rapid loading by GDF of the previously deposited water-rich meltwater plumites, thus resulting in increased pore pressure development. We find that thickness of meltwater plumites deposits exerts a major control on the number and volume of submarine landslides.

83

reviewers whose comments and suggestions helped to improve our paper.

Appendix A. Supplementary material

Supplementary material related to this article can be found at http://dx.doi.org/10.1016/j.quascirev.2015.10.002.

References

Akimova, A., Schauer, U., Danilov, S., Núñez-Riboni, I., 2011. The role of the deep mixing in the Storfjorden shelf water plume. Deep Sea Res. Part I Oceanogr. Res. Pap. 58, 403–414. http://dx.doi.org/10.1016/j.dsr.2011.02.001.

Andersen, E.S., Dokken, T.M., Elverhøi, A., Solheim, A., Fossen, I., 1996. Late Quaternary sedimentation and glacial history of the western Svalbard continental margin. Mar. Geol. 133, 123–156.

Batchelor, C.L., Dowdeswell, J.A., Pietras, J.T., 2013. Seismic stratigraphy, sedimentary architecture and palaeo-glaciology of the Mackenzie Trough: evidence for two Quaternary ice advances and limited fan development on the western Canadian Beaufort Sea margin. Quat. Sci. Rev. 65, 73–87. http://dx.doi.org/10.1016/j.quascirev.2013.01.021.

Bjarnadóttir, L.R., Rüther, D.C., Winsborrow, M.C.M., Andreassen, K., 2013. Grounding-line dynamics during the last deglaciation of Kveithola, W Barents Sea, as revealed by seabed geomorphology and shallow seismic stratigraphy. Boreas 42, 84–107. http://dx.doi.org/10.1111/j.1502-3885.2012.00273.x.

Bryn, P., Berg, K., Stoker, M., Haflidason, H., Solheim, A., 2005. Contourites and their relevance for mass wasting along the Mid-Norwegian Margin. Mar. Petroleum Geol. 22, 85–96. http://dx.doi.org/10.1016/j.marpetgeo.2004.10.012.

Butt, F.A., Elverhøi, A., Solheim, A., Forsberg, C.F., 2000. Deciphering late cenozoic development of the western Svalbard Margin from ODP Site 986 results. Mar. Geol. 169, 373–390. http://dx.doi.org/10.1016/S0025-3227(00)00088-8.

Cuffey, K.M., Conway, H., Gades, A.M., Hallet, B., Lorrain, R., Severinghaus, J.P., Steig, E.J., Vaughn, B., White, J.W.C., 2000. Entrainment at cold glacier beds. Geology 28, 351–354. http://dx.doi.org/10.1130/0091-7613(2000)28<351:EACGB>2.0.CO.

Dahlgren, K.I., Vorren, T.O., Stoker, M.S., Nielsen, T., Nygård, A., Petter Sejrup, H., 2005. Late Cenozoic prograding wedges on the NW European continental margin: their formation and relationship to tectonics and climate. Mar. Petroleum Geol. 22, 1089–1110. http://dx.doi.org/10.1016/j.marpetgeo.2004.12.008.

Dimakis, P., Elverhøi, A., Høeg, K., Solheim, A., Harbitz, C., Laberg, J.S., Vorren, T.O., Marr, J., 2000. Submarine slope stability on high-latitude glaciated Svalbard-Barents Sea margin. Mar. Geol. 162, 303–316. http://dx.doi.org/10.1016/S0025-3227(99)00076-6.

Dokken, T.M., Hald, M., 1996. Rapid climatic shifts during isotope stages 2–4 in the Polar North Atlantic. Geology 24, 599–602. http://dx.doi.org/10.1130/0091-7613(1996)024<0599.

Dowdeswell, J.A., Elverhøi, A., 2002. The timing of initiation of fast-flowing ice streams during a glacial cycle inferred from glacimarine sedimentation. Mar. Geol. 188, 3–14.

Dowdeswell, J.A., Elverhøi, A., Spielhagen, R., 1998. Glacimarine sedimentary processes and facies on the Polar North Atlantic margins. Quat. Sci. Rev. 17, 243–272.

Eldholm, O., Sundvor, E., Myhre, A.M., Faleide, J.I., 1984. Cenozoic evolution of the continental margin off Norway and western Svalbard. In: Spencer, A.M. (Ed.), Petroleum Geology of the North European Margin. Springer Netherlands, Dordrecht, pp. 3–18. http://dx.doi.org/10.1007/978-94-009-5626-1.

Elverhøi, A., Svendsen, J.I., Solheims, A., Andersen, E.S., Milliman, J., Mangerud, J., Hooke, R.L., 1995. Late Quaternary sediment yield from the high Arctic Svalbard area. J. Geol. 103, 1–17. http://dx.doi.org/10.1086/629718.

Faleide, J.I., Vdgnes, E., Gudlaugsson, S.T., 1993. Late Mesozoic-Cenozoic evolution of the south-western Barents Sea in a regional rift-shear tectonic setting. Mar. Petroleum Geol. 10, 186–214.

Faleide, J.I., Solheim, A., Fiedler, A., Hjelstuen, B.O., Andersen, E.S., Vanneste, K., 1996. Late Cenozoic evolution of the western Barents Sea-Svalbard continental margin. Glob. Planet. Change 12, 53–74. http://dx.doi.org/10.1016/0921-8181(95)00012-7.

Faleide, J.I., Tsikalas, F., Breivik, A.J., Mjelde, R., Ritzmann, O., Wilson, J., Eldholm, O., 2008. Structure and evolution of the continental margin off Norway and the Barents Sea. Episodes 31, 82–91.

Fiedler, A., Faleide, J.I., 1996. Cenozoic sedimentation along the southwestern Barents Sea margin in relation to uplift and erosion of the shelf. Glob. Planet. Change 12, 75–93. http://dx.doi.org/10.1016/0921-8181(95)00013-5.

Forsberg, C.F., Solheim, A., Jansen, E., Andersen, E.S., 1999. The depositional environment of the Western Svalbard margin during the Late Pliocene and the Pleistocene: sedimentary facies changes at Site 986. Proc. Ocean Drill. Program Sci. Results 162, 233–246. http://dx.doi.org/10.2973/odp.proc.sr.162.1999.

Gales, J.A., Larter, R.D., Mitchell, N.C., Dowdeswell, J.A., 2013. Geomorphic signature of Antarctic submarine gullies: implications for continental slope processes. Mar. Geol. 337, 112–124. http://dx.doi.org/10.1016/j.margeo.2013.02.003.

Hampel, A., Hetzel, R., Maniatis, G., Karow, T., 2009. Three-dimensional numerical modeling of slip rate variations on normal and thrust fault arrays during ice cap growth and melting. J. Geophys. Res. 114, B08406. http://dx.doi.org/10.1029/2008JB006113.

Hao, Q., Wang, L., Oldfield, F., Peng, S., Qin, L., Song, Y., Xu, B., Qiao, Y., Bloemendal, J., Guo, Z., 2012. Delayed build-up of Arctic ice sheets during 400,000-year minima in insolation variability. Nature 490, 393–396. http://dx.doi.org/10.1038/nature11493.

Hesse, R., Khodabakhsh, S., Klaucke, I., Ryan, W.B.F., 1997. Asymmetrical turbid surface-plume deposition near ice-outlets of the Pleistocene Laurentide ice sheet in the Labrador Sea. Geo-Marine Lett. 17, 179–187. http://dx.doi.org/10.1007/s003670050024.

Hillenbrand, C.-D., Baesler, A., Grobe, H., 2005. The sedimentary record of the last glaciation in the western Bellingshausen Sea (West Antarctica): implications for the interpretation of diamictons in a polar-marine setting. Mar. Geol. 216, 191–204. http://dx.doi.org/10.1016/j.margeo.2005.01.007.

Hjelstuen, B.O., Elverhøi, A., Faleide, J.I., 1996. Cenozoic erosion and sediment yield in the drainage area of the Storfjorden Fan. Glob. Planet. Change 12, 95–117. http://dx.doi.org/10.1016/0921-8181(95)00014-3.

Hjelstuen, B., Eldholm, O., Faleide, J., 2007. Recurrent Pleistocene mega-failures on the SW Barents Sea margin. Earth Planet. Sci. Lett. 258, 605–618. http://dx.doi.org/10.1016/j.epsl.2007.04.025.

Jakobsson, M., Mayer, L., Coakley, B., Dowdeswell, J.A., Forbes, S., Fridman, B., Hodnesdal, H., Noormets, R., Pedersen, R., Rebesco, M., Schenke, H.W., Zarayskaya, Y., Accettella, D., Armstrong, A., Anderson, R.M., Bienhoff, P., Camerlenghi, A., Church, I., Edwards, M., Gardner, J.V., Hall, J.K., Hell, B., Hestvik, O., Kristoffersen, Y., Marcussen, C., Mohammad, R., Mosher, D., Nghiem, S.V., Pedrosa, M.T., Travaglini, P.G., Weatherall, P., 2012. The International Bathymetric Chart of the Arctic Ocean (IBCAO) version 3.0. Geophys. Res. Lett. 39 http://dx.doi.org/10.1029/2012GL052219 n/a–n/a.

Jessen, S.P., Rasmussen, T.L., Nielsen, T., Solheim, A., 2010. A new Late Weichselian and Holocene marine chronology for the western Svalbard slope 30,000–0 cal years BP. Quat. Sci. Rev. 29, 1301–1312. http://dx.doi.org/10.1016/j.quascirev.2010.02.020.

King, E.L., Haflidason, H., Sejrup, H.P., Løvlie, R., 1998. Glacigenic debris flows on the North Sea Trough Mouth Fan during ice stream maxima. Mar. Geol. 152, 217–246.

Knies, J., Matthiessen, J., Vogt, C., Laberg, J.S., Hjelstuen, B.O., Smelror, M., Larsen, E., Andreassen, K., Eidvin, T., Vorren, T.O., 2009. The Plio-Pleistocene glaciation of the Barents Sea–Svalbard region: a new model based on revised chronostratigraphy. Quat. Sci. Rev. 28, 812–829. http://dx.doi.org/10.1016/j.quascirev.2008.12.002.

Laberg, J.S., Vorren, T.O., 1995. Late Weichselian submarine debris flow deposits on the Bear Island Trough Mouth Fan. Mar. Geol. 127, 45–72. http://dx.doi.org/10.1016/0025-3227(95)00055-4.

Laberg, J.S., Vorren, T.O., 1996a. The Middle and Late Pleistocene evolution of the Bear Island Trough Mouth Fan. Glob. Planet. Change 12, 309–330.

Laberg, J.S., Vorren, T.O., 1996b. The glacier-fed fan at the mouth of Storfjorden trough, western Barents Sea: a comparative study. Geol. Rundsch. http://dx.doi.org/10.1007/BF02422239.

Laberg, J.S., Vorren, T.O., 2000. The Trænadjupet Slide, offshore Norway – morphology, evacuation and triggering mechanisms. Mar. Geol. 171, 95–114. http://dx.doi.org/10.1016/S0025-3227(00)00112-2.

Laberg, J.S., Forwick, M., Husum, K., 1996. Proceedings of the Ocean Drilling Program, 162 initial reports. Proc. Ocean Drill. Program 162, 2973. http://dx.doi.org/10.2973/odp.proc.ir.162.1996.

Laberg, J.S., Vorren, T.O., Mienert, J., Evans, D., Lindberg, B., Ottesen, D., Kenyon, N.H., Henriksen, S., 2002. Late Quaternary palaeoenvironment and chronology in the Trænadjupet Slide area offshore Norway. Mar. Geol. 188, 35–60. http://dx.doi.org/10.1016/S0025-3227(02)00274-8.

Laberg, J.S., Andreassen, K., Knies, J., Vorren, T.O., Winsborrow, M., 2010. Late Pliocene-Pleistocene development of the Barents Sea Ice Sheet. Geology 38, 107–110. http://dx.doi.org/10.1130/G30193.1.

Lambeck, K., Purcell, A., Funder, S., Kjær, K., Larsen, E., Möller, P., 2006. Constraints on the Late Saalian to early Middle Weichselian ice sheet of Eurasia from field data and rebound modelling. Boreas 35, 539–575. http://dx.doi.org/10.1080/03009480600781875.

Landvik, J.Y., Bondevik, S., Elverhøi, A., Fjeldskaar, W., Mangerud, J., Salvigsen, O., Siegert, M.J., Svendsen, J.-I., Vorren, T.O., 1998. Last glacial maximum of Svalbard and the Barents Sea Area: ice sheet extent and configuration. Quat. Sci. Rev. 17, 43–75. http://dx.doi.org/10.1016/S0277-3791(97)00066-8.

Lee, H.J., 2009. Timing of occurrence of large submarine landslides on the Atlantic Ocean margin. Mar. Geol. 264, 53–64. http://dx.doi.org/10.1016/j.margeo.2008.09.009.

Lisiecki, L.E., Raymo, M.E., 2005. A Pliocene-Pleistocene stack of 57 globally distributed benthic δ 18 O records. Paleoceanography 20, 1–17. http://dx.doi.org/10.1029/2004PA001071.

Llopart, J., Urgeles, R., Camerlenghi, A., Lucchi, R.G., Mol, B., Rebesco, M., Pedrosa, M.T., 2014. Slope instability of Glaciated Continental Margins: Constraints from Permeability-Compressibility Tests and Hydrogeological Modeling Off Storfjorden, NW Barents Sea. In: Krastel, S., Behrmann, J.-H., Völker, D., Stipp, M., Berndt, C., Urgeles, R., Chaytor, J., Huhn, K., Strasser, M., Harbitz, C.B. (Eds.), Submarine Mass Movements and Their Consequences SE – 9. Springer International Publishing, pp. 95–104. http://dx.doi.org/10.1007/978-3-319-00972-8_9.

Lucchi, R.G., Pedrosa, M.T., Camerlenghi, A., Urgeles, R., De Mol, B., Rebesco, M., 2012. Recent submarine landslides on the continental slope of Storfjorden and Kveithola Trough-Mouth Fans (north west Barents Sea). In: Yamada, Y.,

Kawamura, K., Ikehara, K., Ogawa, Y., Urgeles, R., Mosher, D., Chaytor, J., Strasser, M. (Eds.), Submarine Mass Movements and Their Consequences, Advances in Natural and Technological Hazards Research 31. Springer Netherlands, Dordrecht, pp. 735—745. http://dx.doi.org/10.1007/978-94-007-2162-3.

Lucchi, R.G., Camerlenghi, A., Rebesco, M., Colmenero-Hidalgo, E., Sierro, F.J., Sagnotti, L., Urgeles, R., Melis, R., Morigi, C., Barcena, M.-A., Giorgetti, G., Villa, G., Persico, D., Flores, J.-A., Rigual, A., Pedrosa, M.T., Macri, P., Caburlotto, A., 2013. Postglacial sedimentary processes on the Storfjorden and Kveithola trough mouth fans: significance of extreme glacimarine sedimentation. Glob. Planet. Change 111, 309—326. http://dx.doi.org/10.1016/j.gloplacha.2013.10.008.

Mangerud, J., Svendsen, J.I., 1992. The last interglacial-glacial period on Spitsbergen, Svalbard. Quat. Sci. Rev. 11, 633—664.

Mangerud, J., Dokken, T., Hebbeln, D., Heggen, B., Ingólfsson, Ó., Landvik, J.Y., Mejdahl, V., Svendsen, J.I., Vorren, T.O., 1998. Fluctuations of the Svalbard-Barents sea ice sheet during the last 150000 years. Quat. Sci. Rev. 17, 11—42. http://dx.doi.org/10.1016/S0277-3791(97)00069-3.

Marr, J.G., Elverhøi, A., Harbitz, C., Imran, J., Harff, P., 2002. Numerical simulation of mud-rich subaqueous debris flows on the glacially active margins of the Svalbard-Barents Sea. Mar. Geol. 188, 351—364. http://dx.doi.org/10.1016/S0025-3227(02)00310-9.

Martin, S., Cavalieri, D.J., 1989. Contributions of the Siberian shelf polynyas to the Arctic Ocean intermediate and deep water. J. Geophys. Res. 94, 12725—12738.

Micallef, A., Masson, D.G., Berndt, C., Stow, D. a. V., 2009. Development and mass movement processes of the north-eastern Storegga Slide. Quat. Sci. Rev. 28, 433—448. http://dx.doi.org/10.1016/j.quascirev.2008.09.026.

Noormets, R., Dowdeswell, J.A., Larter, R.D., Ó Cofaigh, C., Evans, J., 2009. Morphology of the upper continental slope in the Bellingshausen and Amundsen Seas — implications for sedimentary processes at the shelf edge of West Antarctica. Mar. Geol. 258, 100—114. http://dx.doi.org/10.1016/j.margeo.2008.11.011.

Ó Cofaigh, C., Taylor, J., Dowdeswell, J.A., Rosell-Melé, A., Kenyon, N.H., Evans, J., Mienert, J., 2002. Sediment Reworking on High-latitude Continental Margins and its Implications for Palaeoceanographic Studies: Insights from the Norwegian-Greenland Sea. Geological Society, London, pp. 325—348. http://dx.doi.org/10.1144/GSL.SP.2002.203.01.17. Special Publications 203.

Ó Cofaigh, C., Taylor, J., Dowdeswell, J.A., Pudsey, C.J., 2003. Palaeo-ice streams, trough mouth fans and high-latitude continental slope sedimentation. Boreas 32, 37—55. http://dx.doi.org/10.1080/03009480310001858.

Ó Cofaigh, C., Andrews, J.T., Jennings, A.E., Dowdeswell, J.A., Hogan, K.A., Kilfeather, A.A., Sheldon, C., 2013. Glacimarine lithofacies, provenance and depositional processes on a West Greenland trough-mouth fan. J. Quat. Sci. 28, 13—26. http://dx.doi.org/10.1002/jqs.2569.

Pedrosa, M.T., Camerlenghi, A., De Mol, B., Urgeles, R., Rebesco, M., Lucchi, R.G., 2011. Seabed morphology and shallow sedimentary structure of the Storfjorden and Kveithola trough-mouth fans (North West Barents Sea). Mar. Geol. 286, 65—81. http://dx.doi.org/10.1016/j.margeo.2011.05.009.

Pirli, M., Schweitzer, J., Paulsen, B., 2013. The Storfjorden, Svalbard, 2008—2012 aftershock sequence: Seismotectonics in a polar environment. Tectonophysics 601, 192—205. http://dx.doi.org/10.1016/j.tecto.2013.05.010.

Quadfasel, D., Rudels, B., Kurz, K., 1988. Outflow of dense water from a Svalbard fjord into the Fram Strait. Deep Sea Res. Part A Oceanogr. Res. Pap. 35, 1143—1150. http://dx.doi.org/10.1016/0198-0149(88)90006-4.

Rasmussen, T.L., Thomsen, E., Ślubowska, M.A., Jessen, S., Solheim, A., Koç, N., 2007. Paleoceanographic evolution of the SW Svalbard margin (76°N) since 20,000 14C yr B.P. Quat. Res. 67, 100—114. http://dx.doi.org/10.1016/j.yqres.2006.07.002.

Raymo, M.E., Jansen, E., Blum, P., Herbert, T.D. (Eds.), 1999. Proc. ODP, Sci. Results, 162. TX (Ocean Drilling Program), College Station. http://dx.doi.org/10.2973/odp.proc.sr.162.1999.

Rebesco, M., Liu, Y., Camerlenghi, A., Winsborrow, M., Laberg, J.S., Caburlotto, A., Diviacco, P., Accettella, D., Sauli, C., Wardell, N., Tomini, I., 2011. Deglaciation of the western margin of the Barents Sea Ice Sheet — a swath bathymetric and sub-bottom seismic study from the Kveithola Trough. Mar. Geol. 279, 141—147. http://dx.doi.org/10.1016/j.margeo.2010.10.018.

Rebesco, M., Pedrosa, M.T., Camerlenghi, A., Lucchi, R.G., Sauli, C., Mol, B. De, Madrussani, G., Urgeles, R., Rossi, G., Böhm, G., 2012. One million years of climatic generated landslide events on the northwestern Barents Sea continental margin. In: Yamada, Y., Kawamura, K., Ikehara, K., Ogawa, Y., Urgeles, R., Mosher, D., Chaytor, J., Strasser, M. (Eds.), Submarine Mass Movements and Their Consequences, Advances in Natural and Technological Hazards Research 31. Springer, Netherlands, Dordrecht, pp. 747—756. http://dx.doi.org/10.1007/978-94-007-2162-3_66.

Rebesco, M., Wåhlin, A., Laberg, J.S., Schauer, U., Beszczynska-Möller, A., Lucchi, R.G., Noormets, R., Accettella, D., Zarayskaya, Y., Diviacco, P., 2013. Quaternary contourite drifts of the Western Spitsbergen margin. Deep Sea Res. Part I Oceanogr. Res. Pap. 79, 156—168. http://dx.doi.org/10.1016/j.dsr.2013.05.013.

Rebesco, M., Laberg, J.S., Pedrosa, M.T., Camerlenghi, A., Lucchi, R.G., Zgur, F.,

Wardell, N., 2014. Onset and growth of trough-mouth fans on the North-Western Barents Sea margin — implications for the evolution of the Barents Sea/Svalbard Ice Sheet. Quat. Sci. Rev. 92, 227—234. http://dx.doi.org/10.1016/j.quascirev.2013.08.015.

Sættem, J., Poole, D.A.R., Ellingsen, L., Sejrup, H.P., 1992. Glacial geology of outer Bjornoyrenna, southwestern Barents Sea. Mar. Geol. 103, 15—51.

Sættem, J., Bugge, T., Fanavoll, S., Goll, R.M., Mork, A., Mork, M.B.E., Smelror, M., Verdenius, J.G., 1994. Marine Cenozoic margin development and erosion of the Barents Sea: core evidence from southwest of Bjornoya. Mar. Geol. 118, 257—281.

Sagnotti, L., Macrì, P., Lucchi, R., Rebesco, M., Camerlenghi, A., 2011. A Holocene paleosecular variation record from the northwestern Barents Sea continental margin. Geochem. Geophys. Geosystems 12, Q11Z33. http://dx.doi.org/10.1029/2011GC003810.

Schauer, U., Fahrbach, E., 1999. A dense bottom water plume in the western Barents Sea: downstream modification and interannual variability. Deep-Sea Res. I 46, 2095—2108. http://dx.doi.org/10.1016/S0967-0637(99)00046-1.

Siegert, M.J., Dowdeswell, J.A., Hald, M., Svendsen, J., 2001. Modelling the Eurasian Ice Sheet through a full (Weichselian) glacial cycle. Glob. Planet. Change 31, 367—385.

Ślubowska-Woldengen, M., Koç, N., Rasmussen, T.L., Klitgaard-Kristensen, D., Hald, M., Jennings, A.E., 2008. Time-slice reconstructions of ocean circulation changes on the continental shelf in the Nordic and Barents Seas during the last 16,000 cal yr B.P. Quat. Sci. Rev. 27, 1476—1492. http://dx.doi.org/10.1016/j.quascirev.2008.04.015.

Spielhagen, R., 2004. Arctic Ocean deep-sea record of northern Eurasian ice sheet history. Quat. Sci. Rev. 23, 1455—1483. http://dx.doi.org/10.1016/j.quascirev.2003.12.015.

Sternberg, R., Aagaard, K., Cacchione, D., Wheatcroft, R., Beach, R., Roach, A., Marsden, M.A., 2001. Long-term near-bed observations of velocity and hydrographic properties in the northwest Barents Sea with implications for sediment transport. Cont. Shelf Res. 21, 509—529. http://dx.doi.org/10.1016/S0278-4343(00)00103-5.

Svendsen, J.I., Alexanderson, H., Astakhov, V.I., Demidov, I., Dowdeswell, J.A., Funder, S., Gataullin, V., Henriksen, M., Hjort, C., Houmark-Nielsen, M., Hubberten, H.W., Ingólfsson, Ó., Jakobsson, M., Kjær, K.H., Larsen, E., Lokrantz, H., Lunkka, J.P., Lyså, A., Mangerud, J., Matiouchkov, A., Murray, A., Möller, P., Niessen, F., Nikolskaya, O., Polyak, L., Saarnisto, M., Siegert, C., Siegert, M.J., Spielhagen, R., Stein, R., 2004. Late Quaternary ice sheet history of northern Eurasia. Quat. Sci. Rev. 23, 1229—1271. http://dx.doi.org/10.1016/j.quascirev.2003.12.008.

Talwani, M., Eldholm, O., 1977. Evolution of the Norwegian-Greenland sea. Geol. Soc. Am. Bull. 88, 969—999. http://dx.doi.org/10.1130/0016-7606(1977)88<969.

Taylor, J., Dowdeswell, J.A., Kenyon, N.H., Ó Cofaigh, C., 2002. Late Quaternary architecture of trough-mouth fans: debris flows and suspended sediments on the Norwegian margin. In: Dowdeswell, J.A., Ó Cofaigh, C. (Eds.), Glacier-influenced Sedimentation on High-latitude Continental Margins. Geological Society, London, pp. 55—71. Special Publications, London.

Tovey, K.N., Paul, M.A., 2001. Modelling self-weight consolidation in Holocene sediments. Bull. Eng. Geol. Environ. 61, 21—33. http://dx.doi.org/10.1007/s100640100126.

Vorren, T.O., Laberg, J.S., 1997. Trough Mouth Fans — Paleoclimate and ice-sheet monitors. Quat. Sci. Rev. 16, 865—881.

Vorren, T.O., Lebesbye, E., Andreassen, K., Larsen, K.-B., 1989. Glacigenic sediments on a passive continental margin as exemplified by the Barents Sea. Mar. Geol. 85, 251—272. http://dx.doi.org/10.1016/0025-3227(89)90156-4.

Vorren, T.O., Lebesbye, E., Larsen, K.B., 1990. Geometry and genesis of the glacigenic sediments in the southern Barents Sea. In: Dowdeswell, J.A., Scourse, J.D. (Eds.), Glacimarine Environments: Processes and Sediments. Geological Society, London, pp. 269—288. http://dx.doi.org/10.1144/GSL.SP.1990.053.01.15. Special Publications.

Vorren, T.O., Landvik, J.Y., Andreassen, K., Laberg, J.S., 2011. Glacial history of the Barents Sea Region. In: Ehlers, J., Gibbard, P.L., Hughes, D. (Eds.), Developments in Quaternary Sciences. Elsevier, pp. 361—372. http://dx.doi.org/10.1016/B978-0-444-53447-7.00027-1.

Williams, D.F., Thunell, R.C., Tappa, E., Rio, D., Raffi, I., 1988. Chronology of the pleistocene oxygen isotope record: 0—1.88 m.y. B.P. Palaeogeogr. Palaeoclimatol. Palaeoecol. 64, 221—240. http://dx.doi.org/10.1016/0031-0182(88)90008-9.

Winsborrow, M.C.M., Andreassen, K., Corner, G.D., Laberg, J.S., 2010. Deglaciation of a marine-based ice sheet: Late Weichselian palaeo-ice dynamics and retreat in the southern Barents Sea reconstructed from onshore and offshore glacial geomorphology. Quat. Sci. Rev. 29, 424—442. http://dx.doi.org/10.1016/j.quascirev.2009.10.001.

Wobus, F., Shapiro, G.I., Huthnance, J.M., Maqueda, M. a. M., Aksenov, Y., 2013. Tidally induced lateral dispersion of the Storfjorden overflow plume. Ocean Sci. 9, 885—899. http://dx.doi.org/10.5194/os-9-885-2013.